PHILOSOPHICAL TRANSACTIONS OF THE ROYAL SOCIETY A MATHEMATICAL, PHYSICAL & ENGINEERING SCIENCES

Global Dynamics of a Planar Mapping Exhibiting Orbits of Periods 1, 2, 3 and no Chaos

A. D. Gilbert

Phil. Trans. R. Soc. Lond. A 1990 **333**, 209-259
doi: 10.1098/rsta.1990.0159

Global dynamics of a planar mapping exhibiting orbits of periods 1, 2, 3 and no chaos

By A. D. Gilbert

Department of Mathematics, James Clerk Maxwell Building, King's Buildings, Mayfield Road, Edinburgh EH9 3JZ, U.K.

Contents

A geometrical analysis of the planar mapping $A:(x,y)\to(y+xy,x)$ is presented. A complete global portrait of the invariant manifolds of A is found, primarily by deductive methods. The behaviour of some manifolds was initially investigated numerically, but theoretical explanations for the observations are given in every case. The most significant features of the mapping A are: that it has periodic points of periods 1, 2 and 3 only; that it possesses no chaotic behaviour; that it has sequences of abutting regions of self-similar structure, and that it exhibits heteroclinic behaviour manifesting itself as exponentially small oscillations in some of the invariant manifolds.

1. Introduction

Mappings of an interval are particularly amenable to graphical methods. This has enabled a good picture to be constructed of various global phenomena occurring

Phil. Trans. R. Soc. Lond. A (1990) **333**, 209–259
Printed in Great Britain

within the orbits of these mappings. Perhaps the most startling of these is the result by Šarkovskii (1964) on the ordering of the periods of periodic solutions of a continuous mapping of an interval or of the real line. An essential component of these phenomena comes from the ability to order points of the interval or real line on which the mapping is defined: the continuity of the mapping imposes various restrictions on the possible orderings of successive iterates, and the existence of certain types of periodic orbit then follows from combinatorial arguments (see, for example, Metropolis *et al.* 1973).

In dimensions greater than one, the ability to order points is lost so that results obtaining for one-dimensional maps are not directly applicable. For dissipative mappings, however, there is the possibility that trajectories will be attracted to some lower-dimensional object in the phase space, and if this happens to be one dimensional, then the results for one-dimensional mappings may be applicable. Examples of this involving period-doubling sequences of bifurcations are mentioned by Collet & Eckman (1980).

Once these essentially one-dimensional phenomena are set aside, there remain to be analysed those that are genuinely higher dimensional. Here the situation is much more complicated and far less well understood. A number of general results exist for Axiom A dynamical systems; these are outlined by Guckenheimer & Holmes (1983). Many systems of interest, however, do not fall into this category, and in the absence of general theories it becomes a valid exercise to examine the behaviour of specific mappings.

In this paper, I present a detailed analysis of the planar mapping

$$A : (x, y) \to (y + xy, x).$$

This first arose in connection with a problem concerning a recurrence relation, described below, but its wider interest as a planar mapping soon became apparent. The results of my analysis show that the mapping A has points of periods 1, 2 and 3 only, that it has no behaviour that could be described as chaotic, that it has sequences of abutting regions of self-similar structure and that it exhibits heteroclinic behaviour. Such behaviour is widely at variance with the behaviour of one-dimensional maps mentioned above (and also examples of planar maps described elsewhere, e.g. Hénon's (1976) map).

The mapping A has features that undoubtedly make it rather curious: the squared map $B = A^2$ satisfying

$$B(x, y) = (x + xy + x^2 y, y + xy),$$

which we study in detail below, has whole lines of fixed points, and also compresses certain curves, which we call singular curves to points. These properties play a vital role in the structure of the phase portrait of A, and at present it remains an open question whether or not there is a class of perturbations under which these features are stable. It is clear that they are not stable under arbitrary smooth perturbations, since, for example, near the origin the mapping could be perturbed at arbitrarily high order so that it became the exact time-1 map of a flow, and for these, heteroclinic behaviour is not possible. This point is elaborated in §2.

In §2 a picture of local invariant manifolds is presented, and from these the importance of the singular curves emerges. In §3, the nature of these curves and their preimages is obtained, and it becomes apparent that the preimages exhibit approximate period 3 behaviour. This behaviour is analysed in §4. It emerges that there is precisely one period 3 orbit and the nature of these points regarded as fixed

points of B^3 (and in fact A^3) and their invariant manifolds is elucidated. From this, the nature of all preimages of the singular curves is then determined. In §5, the disposition of the preimages of the singular curves is used to explain various distinct types of behaviour in the structure of invariant manifolds, and to start to build up a global picture of these manifolds. This process is continued in §6 and the result is the complete global portrait of the invariant manifolds in the plane. Finally, we use this to substantiate the claim that there are periodic orbits of periods 1, 2 and 3 only.

The results and methods presented in this paper are very geometric in character. A computer was used at times to examine behaviour, but it has always proved possible to give a cogent theoretical explanation of the observations, rather than mere descriptions of results obtained numerically. Furthermore, all the detailed results obtained in §§5 and 6 were predicted theoretically, and the computer only used as a tool to draw the various curves accurately. Certain results have been established rigorously, but some, while plausible, remain no more than conjecture. I have tried to indicate the status of the various results throughout the text.

The original problem concerning a recurrence relation, posed by Grossman (1986), is that of finding all $u \in \mathbb{R}$ for which the sequence $\{u_n\}$ satisfying

$$u_{n+2} = u_n/(1+u_{n+1}), \quad n \geqslant 0,$$
$$u_0 = 1, \quad u_1 = u$$

converges to a limit. The existence and uniqueness of u was established analytically by Janssen & Tjaden (1987), who then compute u by a repeated section search procedure. However, this problem has a nice reformulation in terms of the mapping B, namely, that of finding all intersection points of the unstable manifold of the origin (found to be unique in §2) with the line $x = 1$. This intersection is easily seen to exist and to be unique from the nature of B, and in consequence, the approach through mappings now provides a constructive method for the determination of u.

2. Fixed points and period 2 points

The origin is the only fixed point of A. The eigenvalues of the linearized map DA at the origin are $\lambda = 1$ and $\lambda = -1$ with corresponding eigenvectors $(1, 1)$ and $(1, -1)$ respectively. As both eigenvalues have unit modulus, a local analysis of invariant manifolds must be of second order or higher, given below.

Restricted to the axes, $xy = 0$, A reduces to

$$A : (x, y) \mapsto (y, x).$$

Thus A merely reflects the axes in the line $y = x$, so that every point of the axes is a period 2 point of A. For the calculation of the corresponding invariant manifolds of A^2, it is more convenient to regard each point on the axis as a fixed point of the mapping:

$$B = A^2 \quad \text{where} \quad B : (x, y) \mapsto (x + xy + x^2 y, y + xy).$$

B has no other fixed points, so that the axes with the origin excluded give all the (strictly) period 2 points of A.

The eigenvalues of DB at $(x_0, 0)$ are $\lambda = 1$ and $\lambda = 1 + x_0$ with eigenvectors $(1, 0)$ and $(1 + x_0, 1)$ respectively. The eigenvalue $\lambda = 1$ and its eigenvector $(1, 0)$ are direct consequences of all points on the x-axis being fixed points. Thus the stability of such a point under the linearized mapping is completely determined by the eigenvalue $\lambda = 1 + x_0$. For $|1 + x_0| < 1 (> 1)$, the centre-and-stable (centre-and-unstable) manifold theorems (Shub 1987) assure us of the existence of a centre manifold tangent to the

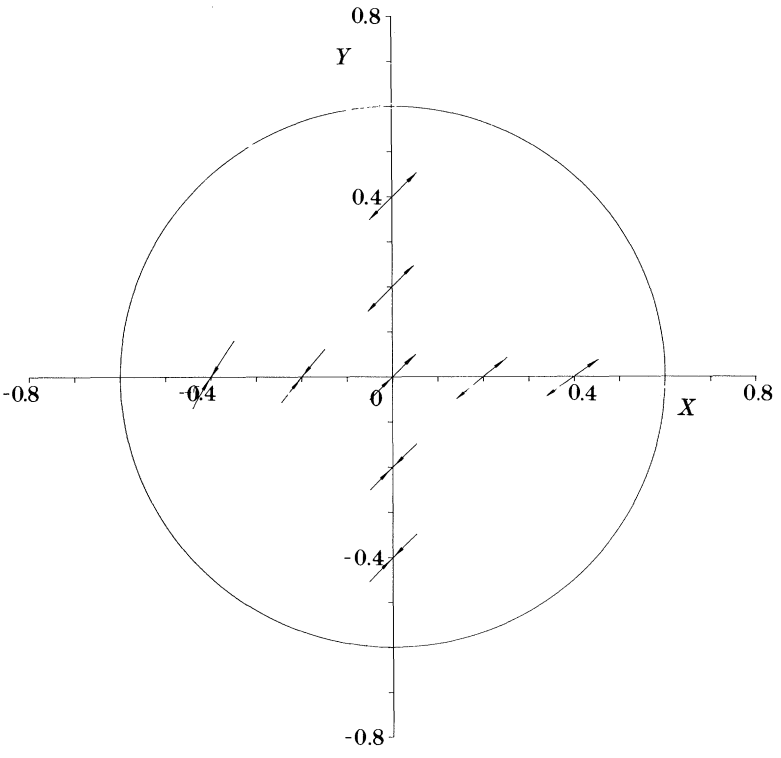

Figure 1. Local stable and unstable manifolds of fixed points of B in a neighbourhood of the origin.

x-direction at $(x_0, 0)$ and also of the existence of a unique stable (unstable) manifold tangent to the direction $(1+x_0, 1)$ at $(x_0, 0)$. The x-axis itself is a centre manifold for the fixed point $(x_0, 0)$, and because every point of the x-axis is fixed under B, there is precisely no motion at all in this centre manifold under iteration by B. Thus stable (unstable) behaviour asymptotic to the fixed point $(x_0, 0)$ under forward iteration is confined to the one-dimensional stable (unstable) manifold of the fixed point $(x_0, 0)$. Similar considerations apply to the fixed point $(0, y_0)$, where the eigenvalues are $\lambda = 1$ and $\lambda = 1+y_0$ with eigenvectors $(0, 1)$ and $(1, 1)$ respectively. The exceptional fixed points, where the linearized analysis above cannot be assumed to yield an approximation to the actual structures of local manifolds, are the origin and the points $(-2, 0)$ and $(0, -2)$. A more detailed analysis of these follows below. However, we observe first that, under the mapping A, a neighbourhood of $(0, -2)$ is mapped diffeomorphically onto a neighbourhood of $(-2, 0)$ and that furthermore under the mapping A, a B-invariant structure is mapped onto a B-invariant structure (since $B = A^2$). Thus it suffices to consider a neighbourhood of $(0, -2)$ alone.

2.1. *Behaviour near* $(0, 0)$

In a sufficiently small neighbourhood N of the origin (O), the linear analysis shows that the fixed points of B within N, apart from O, have local stable and unstable manifolds as sketched in figure 1. A higher order calculation shows that the local stable or unstable manifold emanating from $(0, y_0)$ is described by

$$W(0, y_0): y - y_0 = x + a_2 x^2 + a_3 x^3 + O(x^4),$$

where $a_2 = -1/(2+y_0)$ and $a_3 = (3+2y_0)/(2+y_0)(3+3y_0+y_0^2)$ for $y_0 \neq 0, -2$. For the origin, a separate calculation is required. This involves approximating the mapping B in a sufficiently small neighbourhood of O to cubic order by the time-1 map of the differential equation system

$$\begin{bmatrix} \dot{x} \\ \dot{y} \end{bmatrix} = \begin{bmatrix} xy + \frac{1}{2}xy(x-y) \\ xy - \frac{1}{2}xy(x+y) \end{bmatrix}.$$

Division of the right-hand side by xy yields a non-singular vector field and hence the existence of a unique invariant manifold given by the above expression for $W(0, y_0)$ with y_0 set to zero. Additionally if δ is a suitably chosen coordinate along this local manifold emanating from the origin, we may show that under the mapping B

$$B: \delta \to \delta + \delta^2 + O(\delta^3),$$

so that the origin repels nearby points of $W(\mathrm{O})$ in the first quadrant and attracts them in the third quadrant.

Figure 1 suggests the possibility that in the neighbourhood N of O, the behaviour of manifolds in the first and third quadrants differs from that in the second and fourth: in the former, following the manifolds away from their fixed points leads out of N; in the latter, following the manifolds leads from the positive y (or x) axis towards the negative x (or y) axis. This picture is substantiated below and is illustrated in figure 2*f*. This verification is achieved in two stages. First, for each invariant manifold in N a trapping region is constructed, roughly locating the manifold. Secondly, to establish the motion induced by the mapping and the foliation of various sectors of the plane, a technique somewhat akin to the use of Liapunov functions for ordinary differential equations is used. Initially we consider the invariant manifolds emanating from the y-axis only. Such manifolds are partitioned into four sets S_i, where S_i comprises all those manifolds restricted to N which enter the ith quadrant, $i = 1, 2, 3, 4$. N is restricted so that all the invariant manifolds in a given set S_i have the same stability. Thus S_1 and S_2 have invariant unstable manifolds only, whereas S_3 and S_4 have stable manifolds only. The invariant manifolds of the origin belong to S_1 and S_3.

The sets S_1, S_2, S_3 and S_4 are now treated separately. For each such set, a trapping region for each invariant manifold restricted to N contained by that set is constructed. These are illustrated in figure 2 and listed in table 1. In the figure, the trapping region is shown bounded by solid curves and its image under B (for the unstable manifolds of S_1 and S_2) or B^{-1} (for the stable manifolds of S_3 and S_4), restricted to N, is shown bordered by broken curves. Next, by applying the mapping A to the trapping regions for the B-unstable manifolds, and A^{-1} to the trapping regions for the B-stable manifolds, we obtain corresponding trapping regions for the invariant manifolds emanating from all the fixed points on the x-axis. If we denote by T_i the set of invariant manifolds emanating from a fixed point on the x-axis into the ith quadrant, restricted to N, then with a slight abuse of notation, we have

$$T_1 = A(S_1) \cap N, \quad T_2 = A^{-1}(S_4) \cap N, \quad T_3 = A^{-1}(S_3) \cap N, \quad T_4 = A(S_2) \cap N,$$

and trapping regions for these sets are also illustrated in figure 2 and listed in table 1. Thus we have roughly located the invariant manifolds of all the fixed points in the neighbourhood N of the origin.

We now examine motion along invariant manifolds and foliation of various sectors by them. Let I be an open interval on one axis or two of the axes meeting at the origin

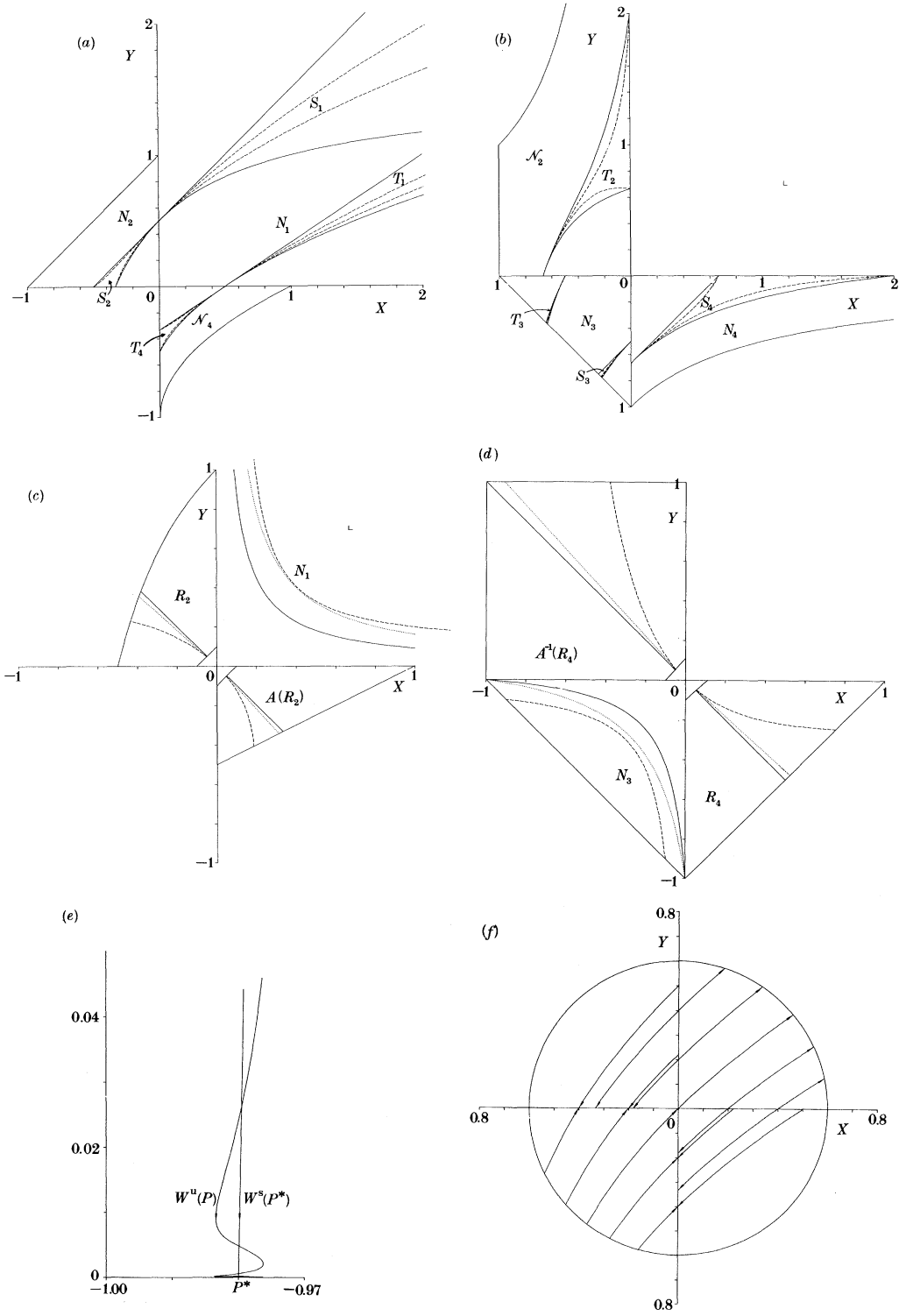

Figure 2*a–f*. For description see opposite.

PHILOSOPHICAL TRANSACTIONS OF THE ROYAL SOCIETY A MATHEMATICAL, PHYSICAL & ENGINEERING SCIENCES

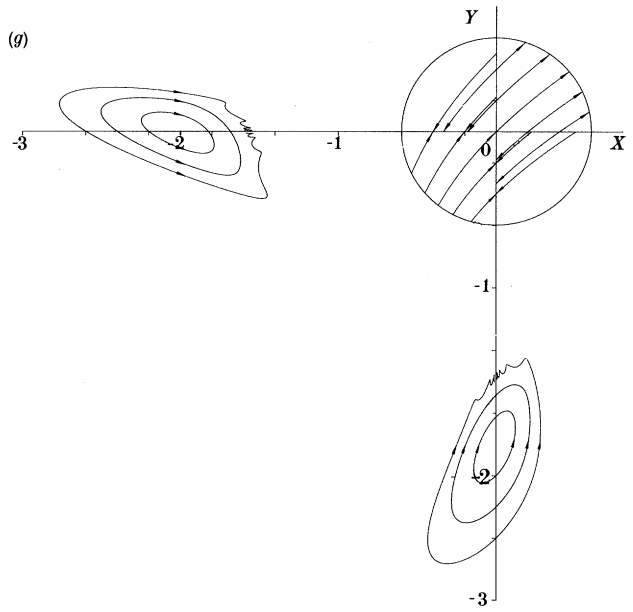

Figure 2. (*a*) Trapping regions (solid lines) and their images under B^{-1} (broken lines) for B-unstable manifolds within the neighbourhoods N_1, N_2 and $\mathcal{N}_4$. (*b*) As (*a*), but for B-stable manifolds. (*c*) Fields of curves C_λ (solid curves), their image under B (broken curve) and intermediate curves $C_{\lambda'}$ (dotted curve) for B-unstable manifolds. (*d*) As (*c*), but for B-stable manifolds. (*e*) Heteroclinic behaviour illustrated by the transversal intersections of $W^{\mathrm{u}}(P), P\colon(0, 2.2)$ with $W^{\mathrm{s}}(P^*), P^*\colon(-0.98, 0)$. (*f*) Invariant manifold structure in a neighbourhood of O. (*g*) Invariant manifold structure near $(0, 0)$, $(0, -2)$ and $(-2, 0)$: those fixed points of B where both eigenvalues of DB have unit modulus.

such that invariant manifolds of the points in the closure of I enter a given quadrant Q and are B-unstable (say). Each of the boundary points of I has a trapping region in Q. Since the unstable manifolds of these boundary points are confined to their trapping regions, the subregion R of Q lying between the two trapping regions contains only points on the unstable manifolds of points of I. To show foliation of R by the unstable manifolds of the points of I, we construct a field F of curves $C_\lambda, \lambda \geqslant 0$ on R with the following properties:

(i) $C_0 = I$;

(ii) as λ increases, C_λ recedes from I;

(iii) between C_λ and its image $B(C_\lambda)$, there exists another member of the field, $C_{\lambda'}$ with $\lambda' > \lambda$ and such that the mapping

$$\beta\colon \lambda \to \lambda'$$

has no positive fixed points.

This field is used as follows. By choosing a sufficiently small λ^*, the curves $C_\lambda, 0 \leqslant \lambda \leqslant \lambda^*$ lie close enough to I that in the region between C_{λ^*} and I, the unstable manifolds of the points of I are approximated as well as we choose by the local formula given earlier. This allows us to conclude that every point of $C_\lambda, 0 \leqslant \lambda \leqslant \lambda^*$ lies on an unstable manifold of some point in I and that C_λ meets every such manifold transversely. Thus the region between C_{λ^*} and I is foliated by manifolds. Applying B and restricting to R, it follows that the region between $B(C_{\lambda^*}) \cap R$ and $I = B(I)$ is also foliated, and by applying B iteratively, that the region of R between $B^n(C_{\lambda^*})$ and I is foliated for all $n \geqslant 0$. But $C_{\beta(\lambda^*)}$ lies between $B(C_{\lambda^*})$ and I, so that $B^{n-1}(C_{\beta(\lambda^*)})$ lies

PHILOSOPHICAL TRANSACTIONS OF THE ROYAL SOCIETY A MATHEMATICAL, PHYSICAL & ENGINEERING SCIENCES

Table 1. *Trapping regions*

set of invariant manifolds S_i, T_i entering quadrant i	neighbourhood $N_i, \mathcal{N}_i$ in quadrant i	upper and lower bounding curves of trapping region
$S_1 = \{W^u(0, y_0) : 0 \leqslant y_0\}$	$N_1 : x, y \geqslant 0$	$C_{1U} : y = y_0 + x, x \geqslant 0$ $C_{1L} : y = y_0 + 1 - 1/(x+1), x \geqslant 0$
$S_2 = \{W^u(0, y_0) : 0 < y_0 < 1\}$	$N_2 : 0 < y < x+1, -1 < x \leqslant 0$	$C_{2U} : y = y_0 + x, -y_0 < x \leqslant 0$ $C_{2L} : y = y_0 + 1 - 1/(1+x), -y_0/(1+y_0) < x \leqslant 0$
$S_3 = \{W^s(0, y_0) : -1 < y_0 \leqslant 0\}$	$N_3 : -x-1 < y \leqslant 0, -1 < x \leqslant 0$	$C_{3U} : y = y_0 + x, (-1-y_0)/2 < x \leqslant 0$ $C_{3L} : y = y_0 + x - 9x^2/8, x^* < x \leqslant 0$, where x^* is the negative root of $y_0 + x - 9x^2/8 = -x - 1$
$S_4 = \{W^s(0, y_0) : -1 < y_0 < 0\}$	$N_4 : -1/(x+1) < y < 0, 0 \leqslant x$	$C_{4U} : y = y_0 + x, 0 \leqslant x < -y_0$ $C_{4L} : y = y_0 + 1 - 1/(x+1), 0 \leqslant x < -y_0/(1+y_0)$
$T_1 = A(S_1) = \{W^u(x_0, 0) : 0 \leqslant x_0\}$	$\mathcal{N}_1 = A(N_1) = N_1$	$\Gamma_{1U} = A(C_{1L}) : x = x_0 + (x_0+1)\, y, y \geqslant 0$ $\Gamma_{1L} : A(C_{1U}) : x = (1+y)\,(x_0+y), y \geqslant 0$
$T_2 = A^{-1}(S_4) = \{W^s(x_0, 0) : -1 < x_0 < 0\}$	$\mathcal{N}_2 = A^{-1}(N_4) : 0 \leqslant y < -1/x, -1 < x < 0$	$\Gamma_{2U} = A^{-1}(C_{4L}) : y = (x - x_0)/(1+x)\,(1+x_0-x), x_0 \leqslant x < 0$ $\Gamma_{2L} = A^{-1}(C_{4U}) : y = (x - x_0)/(1+x), x_0 \leqslant x < 0$
$T_3 = A^{-1}(S_3) = \{W^s(x_0, 0) : -1 < x_0 \leqslant 0\}$	$\mathcal{N}_3 = A^{-1}(N_3) \cap N_3 = N_3$	$\Gamma_{3U} = A^{-1}(C_{3L}) \cap N_3$ $\Gamma_{3L} = A^{-1}(C_{3U}) \cap N_3$
$T_4 = A(S_2) = \{W^u(x_0, 0) : 0 < x_0 < 1\}$	$\mathcal{N}_4 = A(N_2) : 0 < x < (1+y)^2, -1 < y \leqslant 0$	$\Gamma_{4U} = A(C_{2L}) : x = x_0 + (x_0+1)\, y, -x_0/(x_0+1) < y \leqslant 0$ $\Gamma_{4L} = A(C_{2U}) : x = (1+y)\,(x_0+y), -x_0 < y \leqslant 0$

between $B^n(C_{\lambda^*})$ and I, and proceeding inductively, $C_{\beta^n(\lambda^*)}$ lies between $B^n(C_{\lambda^*})$ and I. Thus the foliated region contains $C_{\beta^n(\lambda^*)}$ for all $n \geqslant 0$. But as β has no positive fixed point, it follows that the foliated region contains every field member, and hence the whole of R.

The various regions R and their accompanying fields for the sets of manifolds S_i and T_i are listed in table 2 below. In the construction of these fields we have unioned the sets S_1 and T_1 into a single set of unstable invariant manifolds entering the first quadrant, and similarly S_3 and T_3 into a single set of stable invariant manifolds entering the third quadrant. This cannot be done for the second and fourth quadrants as the adjacent sets of fixed points are of different stabilities. Where sets of stable manifolds are considered, the mapping B must be replaced by B^{-1} in requirement (iii) above. For the sets S_2, T_2, S_4, T_4 a slight refinement of the argument is needed. For $S_2 = \{W^{\mathrm{u}}(0, y_0) : 0 < y_0 < 1\}$, the associated field consists of straight line segments emanating from O into the second quadrant. But a given C_λ and its image under B approach O tangentially, so that there is no possibility of interposing a suitable $C_{\beta(\lambda)}$. Instead, the procedure described above is applied to $\{W^{\mathrm{u}}(0, y_0) : \epsilon < y_0 < 1\}$ for small positive ϵ. As O lies outside the corresponding region R_ϵ, the tangency difficulty does not arise and it is now possible to construct an intermediate field member $C_{\lambda'}$ where $\lambda' = \beta(\lambda, \epsilon)$ now depends on ϵ. We infer, as above, that R_ϵ is foliated, and finally extend the foliated region towards the origin by taking a union over R_ϵ as $\epsilon \to 0$. In figure 2, the region R or $R_\epsilon, \epsilon = 0.1$, along with an example of an associated field member C_λ (solid curve), its image under B and B^{-1} as appropriate (broken curve) and the intermediate field member $C_{\lambda'}$ (dotted curve) are shown for each of the six sets of manifolds in table 2.

We do not intend to prove that the trapping regions and fields listed in the tables have all the properties claimed. We shall, however, illustrate the calculations involved by showing that C_{1L} is indeed a lower bounding curve of the trapping region under B in $N_1 =$ the first quadrant, and that $F_1 : xy = \lambda, \lambda \geqslant 0$ is a suitable field there. The curve C_{1L} is parametrizable as

$$C_{1L} : ((y - y_0)/(y_0 + 1 - y), y), y_0 \leqslant y < y_0 + 1 \quad \text{where} \quad 0 \leqslant y_0,$$

and has image parametrized as

$$B(C_{1L}) : ((y+1)(y - y_0)/(y_0 + 1), y), y_0 < y \leqslant \infty.$$

We wish to show that except at $(0, y_0)$, $B(C_{1L})$ lies strictly above C_{1L}, or equivalently, given the positive slope of these curves, that $B(C_{1L})$ lies strictly to the left of C_{1L} for $y_0 < y < y_0 + 1$. Thus we wish to show that

$$\frac{(y+1)(y - y_0)}{y_0 + 1} < \frac{y - y_0}{y_0 + 1 - y} \quad \text{for} \quad y_0 < y < y_0 + 1 \quad \text{where} \quad 0 \leqslant y_0.$$

This is equivalent to

$$y(y_0 - y) < 0 \quad \text{for} \quad 0 \leqslant y_0 < y < y_0 + 1,$$

which is manifestly true.

Consider now the field $F_1 = \{C_\lambda : xy = \lambda, \lambda \geqslant 0\}$ restricted to N_1, the first quadrant. We note that:

(i) for $\lambda = 0$, C_0 comprises the interval I of fixed points lying along the non-negative x- and y-axes bordering N_1;

PHILOSOPHICAL TRANSACTIONS OF THE ROYAL SOCIETY A MATHEMATICAL, PHYSICAL & ENGINEERING SCIENCES

Table 2. *Fields of curves*

set of manifolds entering quadrant i	corresponding interval of fixed points	region R in quadrant i	field of curves C_λ in $N_i, \mathscr{N}_i$	intermediate curve λ'
$S_1 \cup T_1$	$\{+\text{ve } x\text{-axis}\} \cup \{+\text{ve } y\text{-axis}\}$	$N_1 =$ 1st quadrant	$F_1 : xy = \lambda, \lambda \geqslant 0$	$\lambda(1+2\lambda^{\frac{1}{2}}+2\lambda)$
S_2	$\bigcup_{\epsilon \to 0_+} \{(0, y_0) : \epsilon < y_0 < 1\}$	$R_2 = \bigcup_{0 < y_0 < 1} (C_{2L}) : 0 < y < 2 - 1/(1+x),$ $-\frac{1}{2} < x < 0$	$F_2 : x/y = -\lambda, \lambda \geqslant 0$	$(1+\epsilon)\lambda$
T_2	$\bigcup_{\epsilon \to 0_+} \{(x_0, 0) : -1 < x_0 < -\epsilon\}$	$A^{-1}(R_4) : 0 < y < 1, -1 < x < 0$	$\mathscr{F}_2 : y/x = -\lambda, \lambda \geqslant 0$	$(1+\epsilon)\lambda$
$S_3 \cup T_3$	$\{(x_0, 0) : -1 < x_0 \leqslant 0\} \cup$ $\{(0, y_0) : 1 < y_0 \leqslant 0\}$	N_3	$F_3 : xy/(1+x+y) = \lambda,$ $\lambda \geqslant 0$	$\lambda/(1-2\lambda^{\frac{1}{2}})$ for $0 \leqslant \lambda < \frac{1}{4}$, 2λ for $\frac{1}{4} \leqslant \lambda$
S_4	$\bigcup_{\epsilon \to 0_+} \{(0, y_0) : -1 < y_0 < -\epsilon\}$	$R_4 = \bigcup_{-1 < y_0 < 0} (C_{4U}) : -1 + x < y < 0,\ 0$ $< x < 1$	$F_4 : x/y = -\lambda, \lambda \geqslant 0$	$(1+\epsilon)\lambda$
T_4	$\bigcup_{\epsilon \to 0_+} \{(x_0, 0) : \epsilon < x_0 < 1\}$	$A(R_2) : 0 < x < 1 + 2y, -\frac{1}{2} < y < 0$	$\mathscr{F}_4 : y/x = -\lambda, \lambda \geqslant 0$	$(1+\epsilon)\lambda$

Phil. Trans. R. Soc. Lond. A (1990)

(ii) as λ increases, C_λ recedes from I;
(iii) a point (x, y) on C_λ has image (x', y') under B satisfying

$$x'y' = x(1+y+xy)\,y(1+x) = xy(1+x+y+2xy+x^2y) = \lambda(1+x+y+2\lambda+x\lambda)$$
$$\geqslant \lambda(1+2\lambda^{\frac{1}{2}}+2\lambda)$$

by the arithmetic–geometric inequality and because $x \geqslant 0$. Defining $\lambda' = \beta(\lambda) = \lambda(1+2\lambda^{\frac{1}{2}}+2\lambda)$, it follows that $C_{\lambda'}$ lies between C_λ and $B(C_\lambda)$, and further that $\lambda = 0$ is the only non-negative fixed point of the mapping β.

The calculations summarized above substantiate the suggestion, raised by figure 1, that following the invariant manifolds in a neighbourhood N of O away from their fixed points leads out of N for manifolds in the first and third quadrants, whereas those in the second and fourth quadrants cross from one axis to another. To complete this discussion of behaviour in the neighbourhood N, we must answer the question of how the sets, S_2 and T_4, of unstable manifolds extending forward into the second and fourth quadrants respectively meet the sets T_2 and S_4 of stable manifolds which extend backward into these quadrants. The generic situation is that the manifolds intersect transversely. Let us suppose that this occurs for an unstable manifold in S_2 emanating from a point P on the positive y-axis and a stable manifold in T_2 of a point P^* on the negative x-axis. Then such a point of intersection is a heteroclinic point, and it belongs to an infinite sequence of heteroclinic points. It follows further, that the manifold emanating from P must develop oscillations as it approaches the negative x-axis and ultimately accumulate onto an interval of the negative x-axis. This behaviour is illustrated in figure 2*e*. Similarly the stable manifold $W^{\mathrm{s}}(P^*)$, extended backwards, must develop corresponding oscillations and likewise accumulate onto an interval of the positive y-axis. Behaviour in the 4th quadrant is analogous. Figure 2*e* and related numerical calculations provide strong evidence to support the conclusion that the intersections are transverse, and in §6 we shall advance theoretical evidence to support this conclusion. Additionally, A. M. Davie (personal communication) has used careful asymptotic estimates of the iterates of the mapping extended into $\mathbb{C}^2$ to show that one branch of $W^{\mathrm{u}}(0, y_0)$ accumulates onto an interval of the negative x-axis with width $\sim C\exp(-2\pi^2/y_0)$ as $y_0 \to 0_+$. Numerical calculations of width $\times \exp(2\pi^2/y_0)$ yield values approximated by the expression $11.35+20.80y_0$ with a fractional error bounded by 0.005 for values of y_0 between 1.5 and 2.0. Smaller values of y_0 require more delicate calculations and these were not attempted in view of the strong evidence already described. Assembling all the results found above, we obtain the complete picture of invariant manifolds in a neighbourhood of O illustrated in figure 2*f*.

2.2. *Behaviour near* $(0, -2)$

To analyse behaviour near $(0, -2)$, new coordinates (ξ, η) along the eigenvectors of $DB_{(0,-2)}$ are introduced. Thus

$$\begin{bmatrix} x \\ y+2 \end{bmatrix} = \begin{bmatrix} 1 & 0 \\ 1 & 1 \end{bmatrix} \begin{bmatrix} \xi \\ \eta \end{bmatrix},$$

and in terms of (ξ, η), the mapping B conjugates to $\bar{B}$

$$\bar{B}: \begin{bmatrix} \xi \\ \eta \end{bmatrix} \to \begin{bmatrix} \xi' \\ \eta' \end{bmatrix} = \begin{bmatrix} -\xi \\ \eta \end{bmatrix} + \begin{bmatrix} -\xi^2+\xi\eta \\ 2\xi^2 \end{bmatrix} + \text{cubic terms.}$$

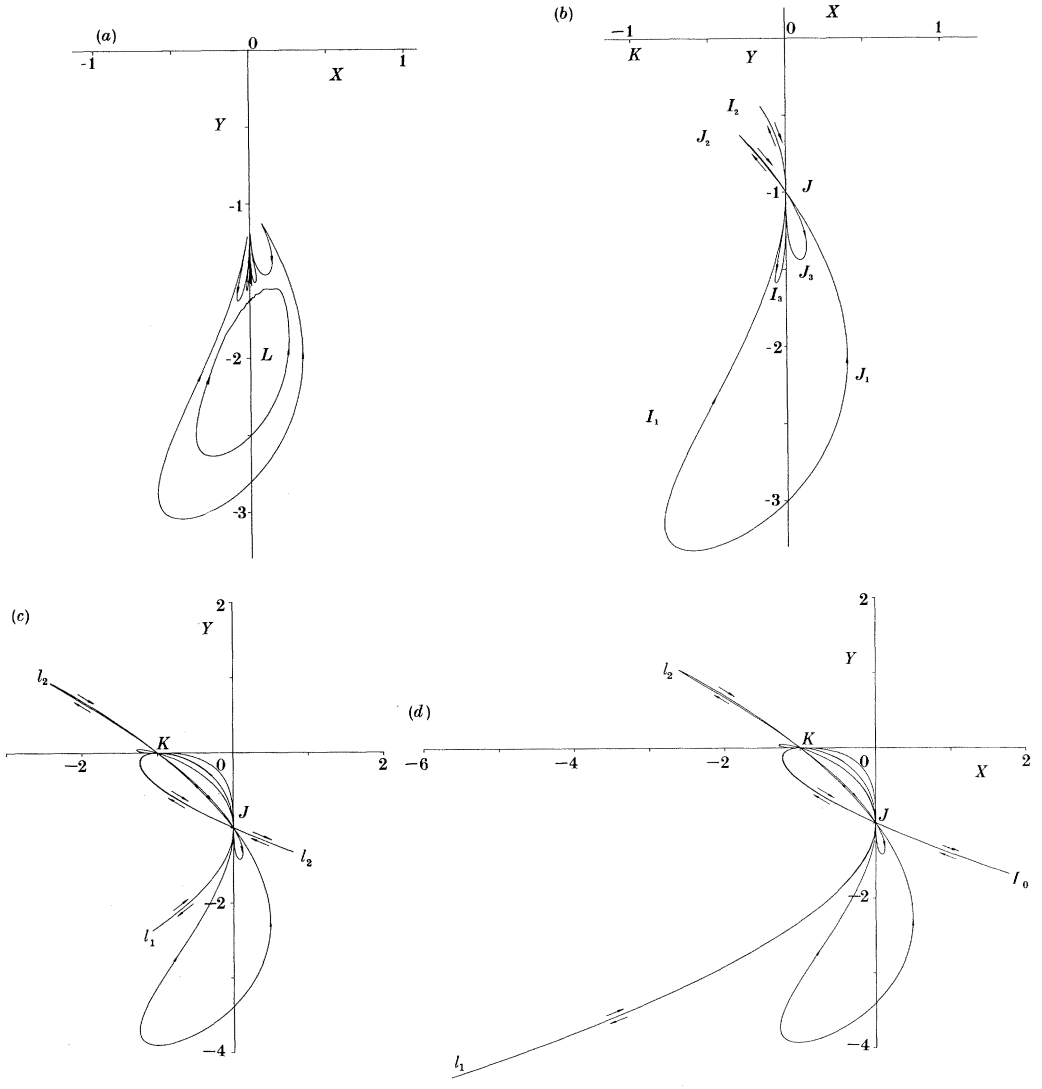

Figure 3. (*a*) Unstable manifolds of $(0, y), y = -2.5$ and -2.8, indicating oscillatory (heteroclinic) behaviour as they approach the y-axis above $y = -2$. (*b*) The first part of $W^u(Y), Y = (0, -3)$, showing repeated passage through $J : (0, -1)$. $W^u(Y)$ is the union of two smooth semi-infinite curves $I_1 I_2 I_3 \ldots$ and $J_1 J_2 J_3 \ldots$, whose subintervals satisfy $I_i = B(J_i)$. The smooth curve $I_1 I_2 I_3 \ldots$ comprises an initial arc I_1, followed by loops $I_2, I_3, \ldots$ based at J which accumulate onto an interval of the negative y-axis. The curve $J_1 J_2 J_3 \ldots$ is similar and accumulates onto the same interval. (*c*) The first part of $W^u(Y)$, $Y = (0, -3.38)$. The loop corresponding to J_2 of figure 3*b* now extends through K into the loop l_2, while that corresponding to I_2 extends through K, then back through J into the loop l_0. Under further iteration, the arcs JK accumulate onto the interval JOK of the axes; the small loops based at J and K tend to small intervals on the axes; the loops l_0, l_1, l_2 generate a finite sequence of similar loops lying close to l_0, l_1, l_2 respectively, but which progressively shorten and ultimately cease. (*d*) The first part of $W^u(Y)$, $Y = (0, -3.4)$. The structure is similar to that of figure 3*c*, except that under further iteration the loops l_0, l_1, l_2 now generate an infinite sequence of similar adjacent loops which progressively lengthen without bound.

Suppression of the orientation reversal in the ξ-direction in the linear approximation is achieved by squaring $\bar{B}$, yielding

$$\bar{B}^2 : \begin{bmatrix} \xi \\ \eta \end{bmatrix} \to \begin{bmatrix} \xi'' \\ \eta'' \end{bmatrix} = \begin{bmatrix} \xi - 2\xi\eta \\ \eta + 4\xi^2 \end{bmatrix} + \text{cubic terms.}$$

From this, there follows

$$2\xi''^2 + \eta''^2 = 2\xi^2 + \eta^2 + \text{quartic terms},$$

so that ellipses $2\xi^2 + \eta^2 =$ constant are approximately invariant under $\bar{B}^2$. In terms of the original coordinates, these approximate invariant curves are the ellipses $3x^2 - 2x(y+2) + (y+2)^2 =$ const., centred on $(0, -2)$, which intersect the y-axis with gradient $+1$, consistent with the direction of the local stable or unstable manifold at the intersection point (a fixed point of B on the y-axis). We shall assume that this family of ellipses does approximate the exact invariant curves in some neighbourhood of $(0, -2)$. Calculations of trapping regions and a suitable field, as performed for the origin, have not been carried out here. Our assumption, however, is supported by numerical calculation, though there is evidence suggesting that the unstable manifold emanating from $(0, y)$ with $y = -2_-$ develops an oscillation as it reapproaches the y axis above $y = -2$, indicative of heteroclinic behaviour, and that its ω-set is a small interval of the y-axis above $y = -2$, not a single point (see figure 3*a*). The amplitude of this oscillation grows as y decreases from -2. Further theoretical evidence for the existence of such an oscillation is given in §5. Because DB is non-singular in a neighbourhood of $(0, -2)$, and locally, B maps points in the third quadrant to points in the fourth quadrant and vice versa, the branches of $W^{\mathrm{u}}(0, y)$, $y = -2_-$ in the third and fourth quadrants are similar geometrically. Thus the approximation of the invariant curves by the above ellipses appears reasonable.

The local stable or unstable manifold of the fixed point $(x_0, 0)$ of B is the image under A of the corresponding local manifold of the fixed point $(0, x_0)$ of B. Because DA is non-singular on the whole of the y-axis, the local manifold at $(x_0, 0)$ is diffeomorphic to that at $(0, x_0)$, and behaviour near all the fixed points of B can now be summarized as in figure 2*g*.

Restricting attention to the fourth quadrant only, figure 2*g* illustrates the entire stable manifold within that quadrant of points $(0, y_0)$ when $y_0 = 0_-$ and -2_+. For $y_0 = 0_-$, these manifolds emanate from fixed points on the positive x-axis, while for $y_0 = -2_+$, they emanate from fixed points $(0, y_1), y_1 = -2_-$. Between $y_0 = 0_-$ and $y_0 = -2_+$, transitional behaviour must occur. To investigate this, unstable manifolds for some points on the negative y-axis below $y = -2$ were computed numerically. These are shown in figure 3. The most noteworthy features are (i) the oscillations in the unstable manifolds of the points $(0, -2.5)$ and $(0, -2.8)$ which occur as these manifolds approach the y-axis above $y = -2$, (ii) the repeated passages through $(0, -1)$ of the unstable manifold of the point $(0, -3)$, (iii) the repeated passages through $(0, -1)$ and $(-1, 0)$ of the unstable manifold of the point $(0, -3.38)$, and (iv) the repeated passages through $(0, -1)$ and $(-1, 0)$ and additionally the development of extremely long narrow loops extending into the second, third and fourth quadrants in the unstable manifold of the point $(0, -3.4)$. A full explanation of these phenomena is given in §5.

3. Singular curves and their preimages

The repeated passages of the B-invariant manifolds through the points $(0,-1)$ and $(-1,0)$ implies that the preimages of these points must lie on these invariant manifolds. Accordingly, the preimages of these points must be analysed. If the mapping $B:(x,y)\to(x',y')$ is written as

$$y'=(1+x)\,y,\quad x'=(1+y')\,x,$$

then $(x',y')=(0,-1)$ implies $(1+x)\,y=-1$ and conversely, whereas $(x',y')=(-1,0)$ implies $x=-1$ and conversely. That is, the preimages of $J:(0,-1)$ and $K:(-1,0)$ are precisely the singular (under B) curves $C:(1+x)\,y=-1$ and $C':x=-1$ respectively. As we shall use this notation throughout, we present it here for easy reference.

point	symbol	preimage under B	symbol
$(0,-1)$	J	curve $(1+x)\,y=-1$	C
$(-1,0)$	K	line $x=-1$	C'

Further preimages under B may be calculated by repeated application of B^{-1}, where

$$B^{-1}\begin{bmatrix}x\\y\end{bmatrix}=\begin{bmatrix}x/(1+y)\\y(1+y)/(1+x+y)\end{bmatrix}.$$

B^{-1} is singular on the lines $\mathscr{L}:y=-1$ and $\mathscr{L}':x+y=-1$. In consequence, a sufficiently short section of curve cutting $\mathscr{L}$ or $\mathscr{L}'$ transversely in a point P, other than J or K, has an image under B^{-1} with two distinct parts which tend to infinity in opposite directions to one another: the curve is effectively 'torn' at P. Under B^{-1}, the point $(x,-1/(x+1))\in C$ is mapped to $(1+x,-1/(1+x)(2+x))$, so that $B^{-1}(C)$ is the curve $y=-1/x(x+1)$. Applying B^{-1} again, the point $(x,-1/x(x+1))\in B^{-1}(C)$ is mapped to

$$\left(\frac{x^2(1+x)}{x^2+x-1},\frac{-(x^2+x-1)}{x(1+x)(x^3+2x^2+x-1)}\right)\in B^{-2}(C).$$

The sequence of curves $C,B^{-1}(C),B^{-2}(C)$ together with the lines $\mathscr{L}$ and $\mathscr{L}'$ is illustrated in figure 4. Similarly, under B^{-1}, the point $(-1,y)\in C'$ maps to $(-1/(1+y),1+y)$, so that $B^{-1}(C')$ is the curve $xy=-1$, while $(-1/y,y)\in B^{-1}(C')$ maps to

$$\left(\frac{-1}{y(y+1)},\frac{y^2(1+y)}{y^2+y-1}\right)\in B^{-2}(C')$$

and the sequence of curves $C',B^{-1}(C'),B^{-2}(C')$ is illustrated in figure 5. The convention $\bar{\alpha}=B^{-1}(\alpha),\bar{\bar{\alpha}}=B^{-1}(\bar{\alpha})$ for points α is used in these figures.

There are broad similarities between figures 4 and 5, so only the former is considered in detail. In figure 4*c*, showing $C,B^{-1}(C)$ and $B^{-2}(C)$, two types of behaviour are apparent, and these suffice to give a complete qualitative description of $B^{-n}(C)$ for all $n\geqslant 0$. There are loops $\bar{\bar{C}}_{\mathrm{b}}\bar{\bar{D}}$, $\bar{A}\bar{\bar{B}}_{\mathrm{a}}$, $\bar{\bar{E}}\bar{\bar{F}}_{\mathrm{a}}$ and $\bar{\bar{G}}_{\mathrm{b}}\bar{\bar{H}}$ lying in the second, third and fourth quadrants only. Each such loop is characterized by having two unbounded portions, both of which recede to infinity in the same direction. We shall call these *infinite loops*. Additionally there are curves such as $\bar{\bar{G}}_{\mathrm{a}}\bar{\bar{F}}_{\mathrm{b}}$ and $\bar{\bar{C}}_{\mathrm{a}}\bar{\bar{B}}_{\mathrm{b}}$, also in the second, third and fourth quadrants only. Each of these has two unbounded portions which recede to infinity in perpendicular directions. We shall call these curves *infinite arcs*.

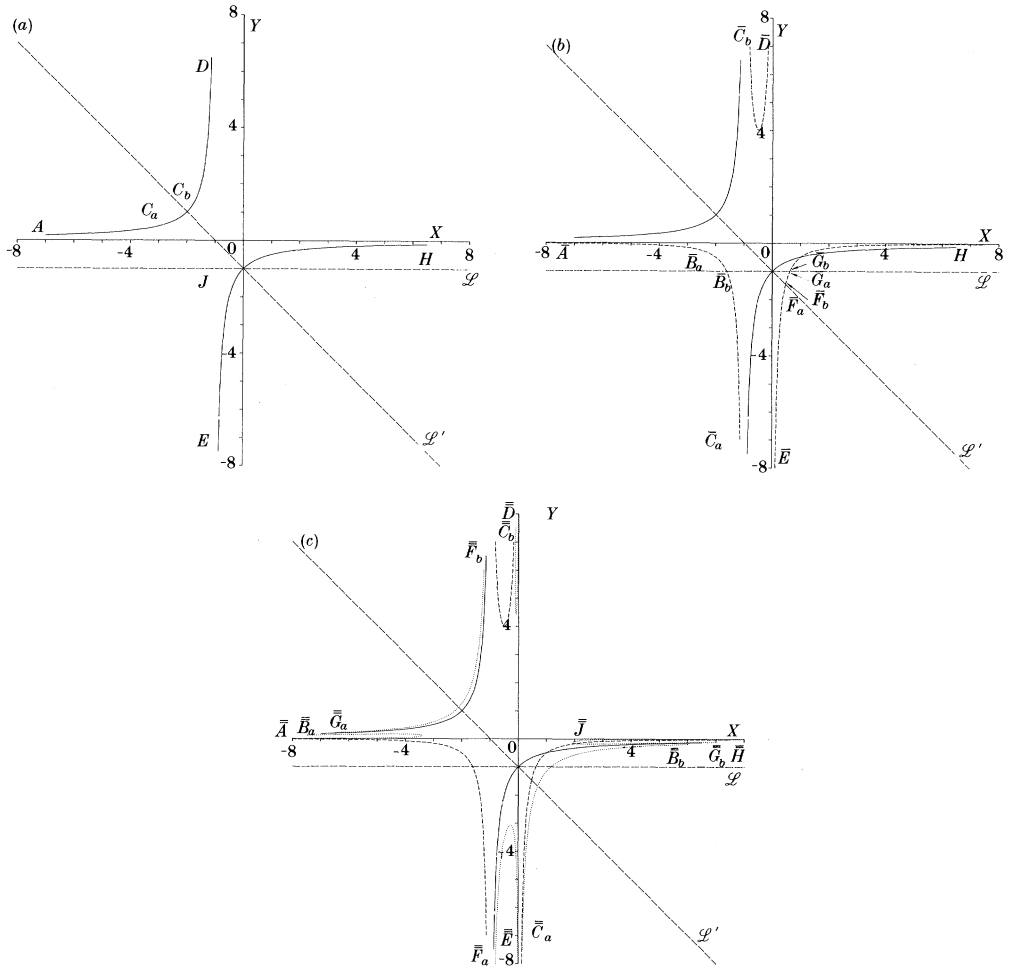

Figure 4. The singular curve $C:(1+x)\,y=-1$ (solid curve (a)) and preimages $B^{-1}(C)$ and $B^{-2}(C)$. $B^{-1}(C)$ is shown broken (b) and $B^{-2}(C)$ is shown dotted (c). Under the preimaging process, intersection points of these curves with the lines $\mathscr{L}$ and $\mathscr{L}'$, other than $J:(0,-1)$, are mapped to infinity. The notation $\bar{A}=B^{-1}(A), \bar{\bar{A}}=B^{-1}(\bar{A})$ etc. is used so that behaviour of various subarcs of these curves under the preimaging process may be followed.

The infinite loops lie close to unbounded intervals of the axes composed of fixed points which attract under B^{-1}. It may be shown that there exist semi-infinite strips adjacent to the axes, containing the loops, which are mapped into themselves under B^{-1} or B^{-2} (for the negative x- and y-axes, where the fixed points are orientation-reversing). Additionally, under repeated iteration by B^{-1}, these strips are attracted towards the axes. Thus the loops map successively into narrower loops and accumulate onto various semi-infinite intervals of the axes. This is summarized in the table below and is illustrated in figure 6. Limiting intervals are shown in figure 7.

loop	limiting interval	
$\bar{G}_b\bar{J}\bar{H}$	$[x_1,\infty)$ of x axis, $x_1=2.3138984$	loops approach from below
$\bar{C}_b\bar{D}$	$[y_1,\infty)$ of y axis, $y_1=4.5240238$	loops approach from left
$\bar{\bar{A}}\bar{B}_a$	$(-\infty,x_0]$ of x axis, $x_0=-3.1801480$	loops alternate above and below axis
$\bar{\bar{E}}\bar{\bar{F}}_a$	$(-\infty,y_0]$ of y axis, $y_0=-2.8592161$	loops alternately left and right of axis

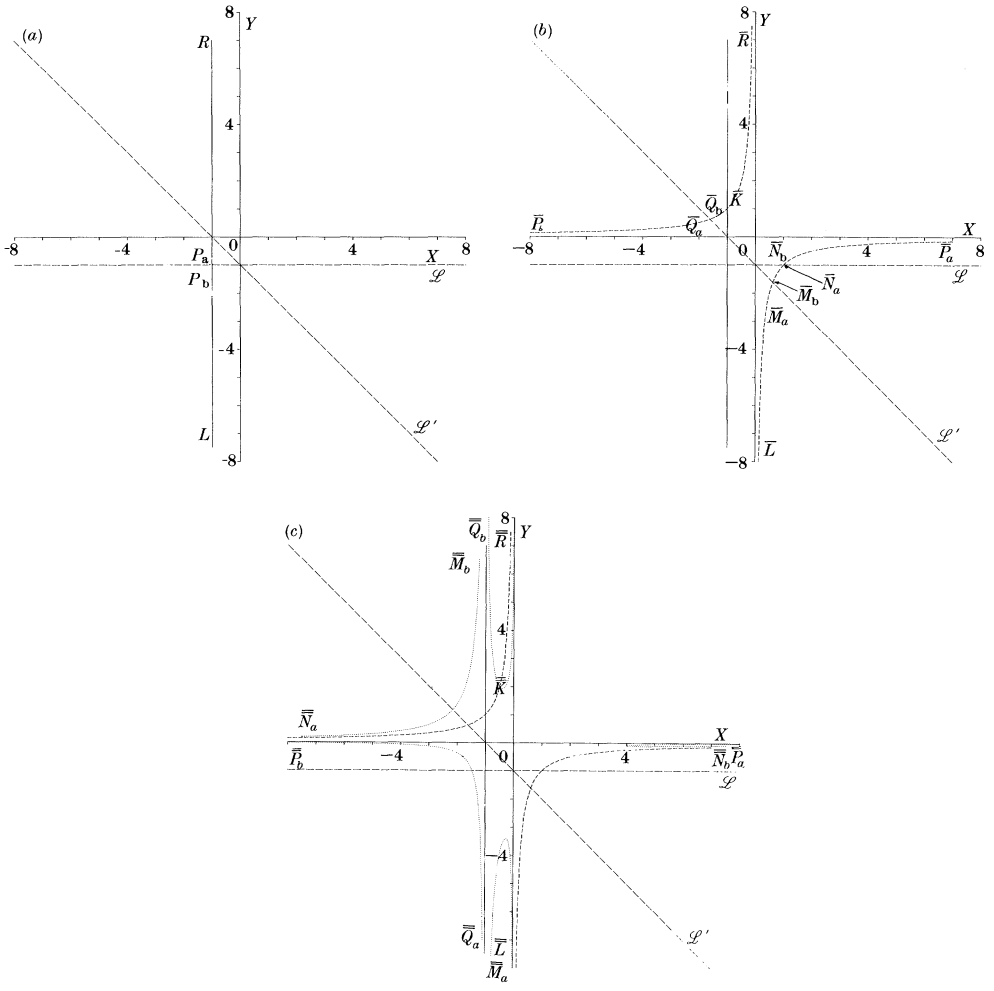

Figure 5. As figure 4 but for the singular curve $C' : x = -1$.

The iterates under B^{-1} of C' yield a qualitatively similar accumulation of loops onto intervals lying along the axes. Thus iterates of the loop $\bar{\bar{N}}_b \bar{\bar{P}}_a$ in figure 5*c* tend towards the interval $[x_1', \infty)$ of the x-axis, where $x_1' = 4.524\,023\,8 = y_1$. The equality between x_1' and y_1 follows simply from reconsidering the map A. The singular curves C and C' are related by

$$C' = A(C),$$

so that $B^{-2}(C') = B^{-2}(A(C)) = A(B^{-2}(C))$, since $B = A^2$. In particular, the loops $\bar{\bar{N}}_b \bar{\bar{P}}_a \subset B^{-2}(C')$ and $\bar{\bar{C}}_b \bar{\bar{D}} \subset B^{-2}(C)$ satisfy $\bar{\bar{N}}_b \bar{\bar{P}}_a = A(\bar{\bar{C}}_b \bar{\bar{D}})$. Now applying B^{-n} yields $B^{-n}(\bar{\bar{N}}_b \bar{\bar{P}}_a) = A(B^{-n}(\bar{\bar{C}}_b \bar{\bar{D}}))$ and, letting $n \to \infty$,

$$\{(x, 0) \,|\, x_1' \leqslant x < \infty\} = A\{(0, y) \,|\, y_1 \leqslant y < \infty\}.$$

But $A(0, y) = (y, 0)$, so that $y_1 = x_1'$. Similarly the other limiting intervals for the curve C' are related to those for the curve C in a fashion illustrated in figure 7 (their displacement from the axes being solely for reasons of clarity).

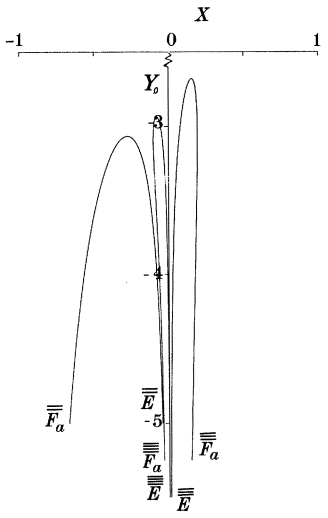

Figure 6. Accumulation of loops in successive preimages of the singular curve C onto an interval of the negative y-axis. Y_0 is the uppermost point of the interval of accumulation.

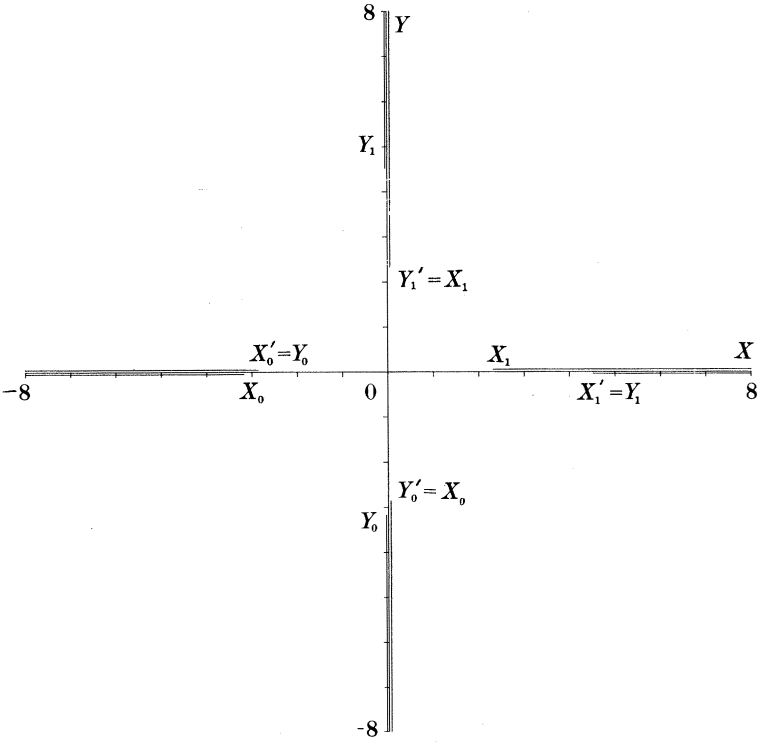

Figure 7. Intervals of accumulation of loops in the preimages of the singular curves C and C'.

Turning again to figure 4*c*, the remaining curves are the infinite arcs, defined above. The principal feature about these curves is that they have an approximate self-replicating property under repeated application of B^{-1}. Consider the curve $\Gamma = \bar{E}\bar{H}$ lying in the fourth quadrant in figure 4*b*. Under B^{-1}, the unbounded portions $\bar{G}_b J\bar{H}$ and $\bar{E}\bar{F}_a$ transform to loops discussed earlier, but the finite are $\bar{F}_b \bar{G}_a$ transforms

to the infinite arc $\bar{\bar{G}}_a \bar{\bar{F}}_b$ shown in figure 4*c*. This curve lies close to the infinite arc $AC_a C_b D$ of figure 4*a* (shown as a solid unlettered curve in figure 4*c*) and this proximity underlies the conjecture advanced below, which is fully supported by numerical evidence. Under application of B^{-1}, $AC_a C_b D$ maps into the two curves shown in figure 4*b*, the infinite loop $\bar{C}_b \bar{D}$ already described, and the arc $\bar{A}\bar{B}_a \bar{B}_b \bar{C}_a$ of the type under discussion. By continuity, the image of $\bar{\bar{G}}_a \bar{\bar{F}}_b$ under B^{-1} can also be expected to be two curves, one close to $\bar{C}_b \bar{D}$ and the other, $\tilde{\Gamma}$ say, close to $\bar{A}\bar{B}_a \bar{B}_b \bar{C}_a$. Applying B^{-1} to $\bar{A}\bar{B}_a \bar{B}_b \bar{C}_a$ yields two further curves, one of which is $\bar{\bar{B}}_b \bar{\bar{C}}_a$ in figure 4*c*, so that we anticipate that $B^{-1}(\tilde{\Gamma})$ consists of two curves, one of which closely approximates $\bar{\bar{B}}_b \bar{\bar{C}}_a$. But $\bar{\bar{B}}_b \bar{\bar{C}}_a$ lies close to $\bar{E}\bar{H}$, which was the curve initially considered. The above sequence, showing the actual preimages of Γ, found by numerical calculation, is illustrated in figure 8. It shows that under $(B^{-1})^3$, the initial curve has indeed approximately replicated itself, and additionally generated the four loops asymptotic to the axes, whose ultimate fate under B^{-1} has already been discussed. The approximate replication of the curve Γ under $(B^{-1})^3$ suggests that under repeated application of $(B^{-1})^3$, the iterates of $\bar{E}\bar{H}$ may accumulate on some curve invariant under $(B^{-1})^3$. Thus it becomes necessary to analyse structures invariant under $(B^{-1})^3$, or equivalently, under B^3.

4. Period 3 behaviour

A point $\boldsymbol{x}$ of period 3 under B satisfies $B^3(\boldsymbol{x}) = \boldsymbol{x}$. Because $B = A^2$, $\boldsymbol{x}$ equivalently satisfies $A^6(\boldsymbol{x}) = \boldsymbol{x}$. By writing $\boldsymbol{x}_n = A^n(\boldsymbol{x})$, it follows that $\{\boldsymbol{x}_n\}$ satisfy

$$\boldsymbol{x}_{n+1} = A\boldsymbol{x}_n, \quad \boldsymbol{x}_{n+6} = \boldsymbol{x}_n.$$

Let $\boldsymbol{x}_n$ have components (x_n, y_n). Then the system is

$$\begin{bmatrix} x_{n+1} \\ y_{n+1} \end{bmatrix} = \begin{bmatrix} (1+x_n)\, y_n \\ x_n \end{bmatrix}, \quad \begin{bmatrix} x_{n+6} \\ y_{n+6} \end{bmatrix} = \begin{bmatrix} x_n \\ y_n \end{bmatrix}$$

and, from the second row, this system is equivalent to

$$x_{n+1} = x_{n-1}(1+x_n), \quad x_{n+6} = x_n,$$

with y_n determined by $y_n = x_{n+1}$. Motivated by the period 6 behaviour of this system, we make a discrete Fourier transform (Strang 1986) by writing

$$x_j = \sum_{\kappa=0}^{5} \frac{\omega^{j\kappa}}{\sqrt{6}} \xi_\kappa, \quad j = 0, 1, \ldots, 5,$$

where $\omega = \exp(\mathrm{i}\pi/3)$. The transformed system is then

$$\xi_\kappa = \omega^{-2\kappa}\xi_\kappa + \frac{1}{\sqrt{6}} \sum_{l=0}^{5} \omega^{-\kappa-l} \xi_l \xi_{\kappa-l}, \quad \kappa = 0, 1, \ldots, 5.$$

The equations for $\kappa = 1, 3, 5$ are respectively

$$-\sqrt{6}\,\bar{\omega}\xi_1 = \xi_0\xi_1 - \xi_3\xi_4, \quad 0 = \xi_1\xi_2 - \xi_4\xi_5, \quad -\sqrt{6}\,\omega\xi_5 = \xi_0\xi_5 - \xi_2\xi_3,$$

from which follows $\sqrt{6}(\omega - \bar{\omega})\xi_1\xi_5 = 0$, so that $\xi_1 = 0$ or $\xi_5 = 0$. Now for a real solution $\{x_j\}$, $\xi_5 = \bar{\xi}_1$, so that both ξ_1 and ξ_5 vanish. From above, there then follows $\xi_3\xi_4 = 0$ and $\xi_2\xi_3 = 0$. If $\xi_3 \neq 0$, then $\xi_2 = \xi_4 = 0$, and the remaining equations reduce to $\xi_0^2 - \xi_3^2 = 0$ so that $\boldsymbol{\xi} = \xi_0(1, 0, 0, \pm 1, 0, 0)^t$, and these correspond to fixed points of B on

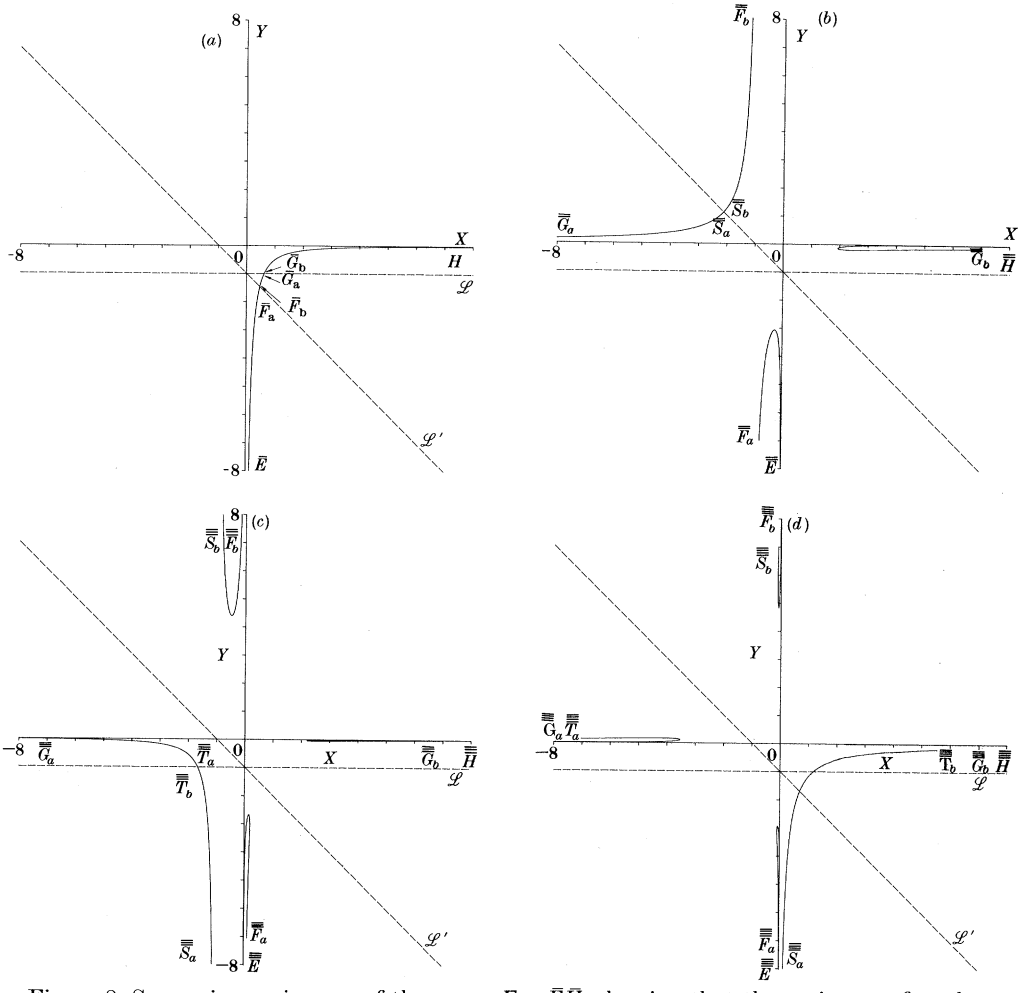

Figure 8. Successive preimages of the curve $\Gamma = \bar{E}\bar{H}$, showing that the preimage after three iterations contains an infinite arc $(\bar{\bar{S}}_a \bar{\bar{T}}_b)$ closely approximating the original curve.

the x- and y-axes. If, however, $\xi_3 = 0$, then by using $\xi_4 = \bar{\xi}_2$ for real $\{x_j\}$, the equations for $\kappa = 0, 2, 4$ reduce to $0 = \xi_0^2 - \xi_2\bar{\xi}_2$ and $-\sqrt{6}(1+\omega)\,\xi_2 = \xi_0\,\xi_2 - \bar{\xi}_2^2$. If $\xi_2 = r\,\mathrm{e}^{\mathrm{i}\theta}$, then $\xi_0 = \pm r$ and $r\,\mathrm{e}^{-3\mathrm{i}\theta} = \sqrt{6}(1+\omega) \pm r$. By taking moduli of the latter, there follows $r = \mp\sqrt{6}$, whence $\mathrm{e}^{-3\mathrm{i}\theta} = \mp\mathrm{e}^{\mathrm{i}\pi/3}$. Hence $\xi_2 = r\,\mathrm{e}^{\mathrm{i}\theta} = \sqrt{6}\exp(\mathrm{i}(-\frac{1}{9}\pi + \frac{2}{3}\kappa\pi))$ for either choice of signs, and $\xi_0 = -\sqrt{6}$. Reconstructing the solution $\{x_j\}$ shows that there are just three distinct values expressible as $x_n = -1 + 2\cos(-\frac{1}{9}\pi - \frac{2}{3}n\pi) = x_{n+3}$. Hence there are precisely three strictly period 3 points $\{P_0, P_1, P_2\}$ of B (and A) expressible as

$$P_n : \boldsymbol{x}_{2n} = (-1 + 2\cos(-\tfrac{1}{9}\pi + \tfrac{2}{3}n\pi),\ -1 + 2\cos(\tfrac{5}{9}\pi + \tfrac{2}{3}n\pi)),$$

which satisfy $P_{n+1} = B(P_n) = A^2(P_n) = A^{-1}(P_n)$.

The stability or otherwise of the period 3 points is examined by evaluating $D(B^3)$ at P_0, for example. By using $DB^3(\boldsymbol{x}_0) = DB(\boldsymbol{x}_4)\,DB(\boldsymbol{x}_2)\,DB(\boldsymbol{x}_0)$, one finds that

$$D(B^3)(\boldsymbol{x}_0) = \begin{bmatrix} 64 + 9c + 9\sqrt{3}s & -36 + 9c + 27\sqrt{3}s \\ -9c + 27\sqrt{3}s & 19 - 9c - 9\sqrt{3}s \end{bmatrix},$$

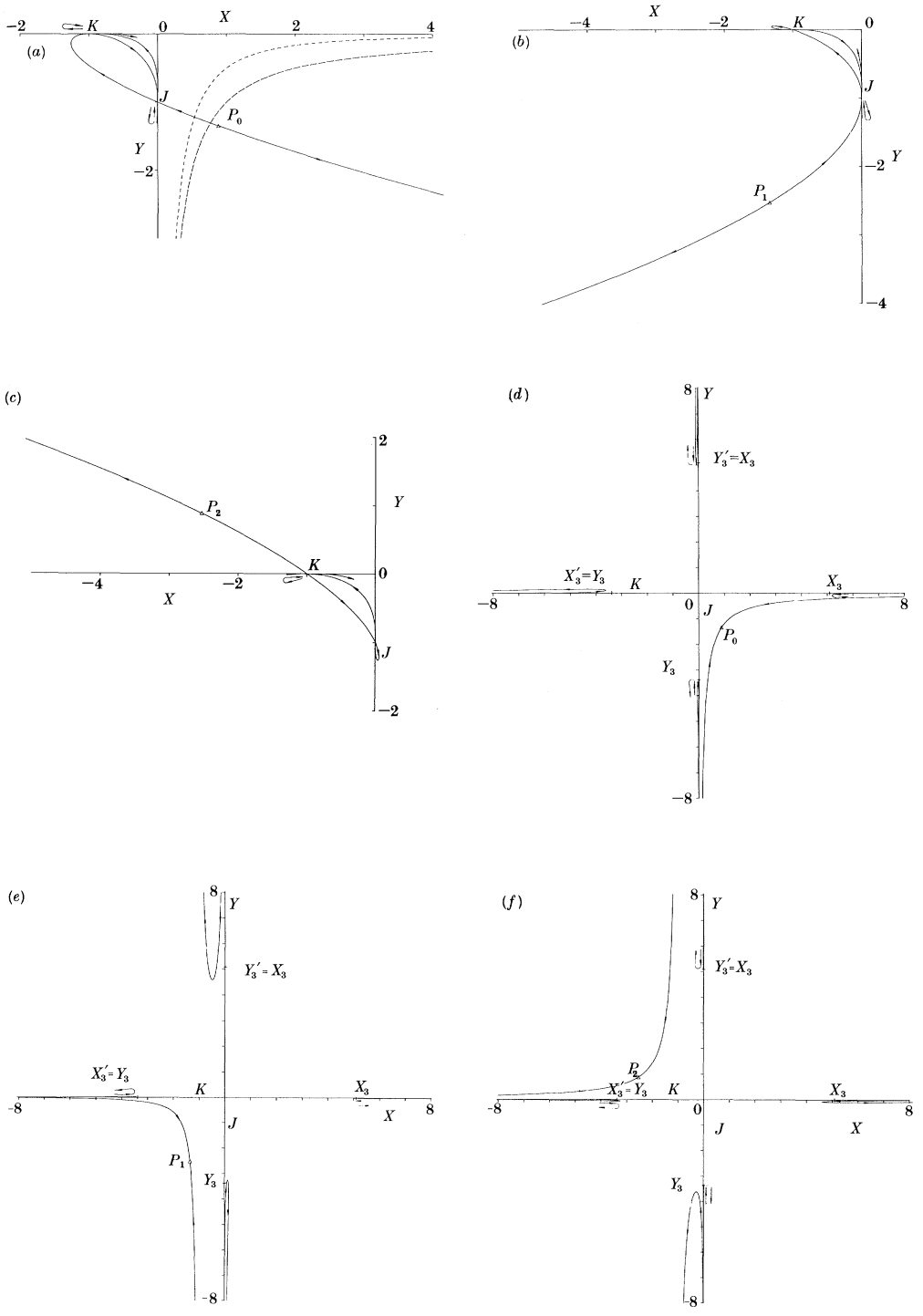

Figure 9. Unstable ((*a*), (*b*), (*c*)) and stable ((*d*), (*e*), (*f*)) manifolds of the points P_0, P_1, P_2 regarded as fixed points of B^3. Very narrow loops based at J and K have both their sense of description and their disposition relative to the y- and x-axis respectively indicated by the 'hairpin' symbols.

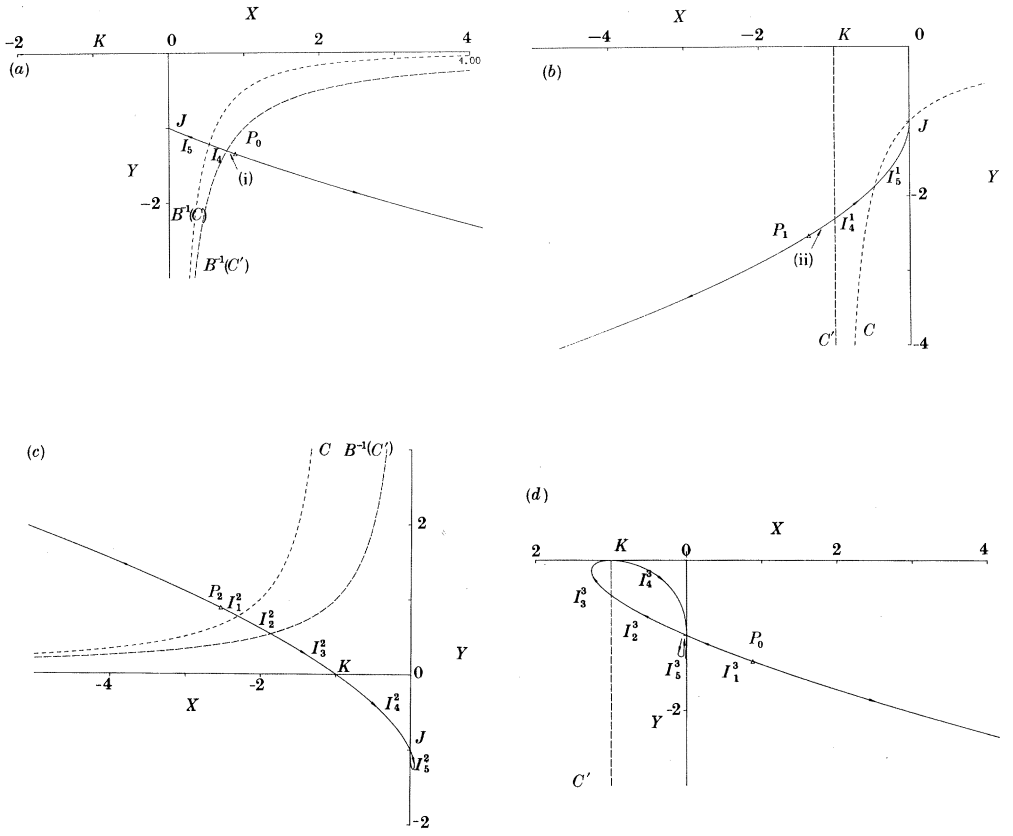

Figure 10. Development of $W^u(P_0)$ (solid curve) under iteration by B. Also shown, where relevant, are the singular curves C and its preimages (broken line, short dash) and C' and its preimages (broken line, long dash). (i) $I_1 \cup I_2 \cup I_3$; (ii) $I_1' \cup I_2' \cup I_3'$.

where $c = \cos(-\frac{1}{9}\pi)$, $s = \sin(-\frac{1}{9}\pi)$. This matrix has a determinant 1 and a trace of 83, so that the eigenvalues are approximately $\lambda = 83$ and $\lambda = 1/83$. The eigenvectors of this matrix enable numerical computation of the stable and unstable manifolds of the period 3 points, and these are shown in figure 9.

Figure 9*a* shows part of $W^u(P_0)$, the unstable manifold of P_0, regarded as a fixed point of B^3. The structure can be understood by means of figure 10. Accepting that curves $B^{-1}(C'): y = -1/x$ and $B^{-1}(C): y = -1/x(x+1)$, and their iterates under B^{-3} have intersection points with $W^u(P_0)$ which accumulate onto P_0, it follows that $W^u(P_0)$ must make infinitely many passages through $J:(0,-1)$ and $K:(-1,0)$. Consider iteration under B^3 of the portion P_0J of $W^u(P_0)$ in figure 10*a*. It is necessary to subdivide P_0J into intervals I_j, and we use the notation $I_j^n = B^n(I_j)$. Under B, P_0 maps to P_1, J remains fixed and intersections with $B^{-1}(C'): y = -1/x$ and $B^{-1}(C)$: $y = -1/x(x+1)$ map to intersections with $C': x = -1$ and $C: y = -1/(x+1)$ respectively. This is illustrated in figure 10*b*. Under a further application of B, the curve shown in figure 10*c* results: the portion of the curve between P_1 and $C': x = -1$ maps to the portion of curve P_2K; the portion of curve I_4^1 in figure 10*b* transforms to the arc KJ labelled I_4^2 in figure 10*c*; and I_5^1 of figure 10*b* is transformed into the loop I_5^2 in figure 10*c* because the entire curve $C: y = -1/(x+1)$ is mapped to the point J

under B. In figure 10c, P_2K intersects first with $C: y = -1/(x+1)$, then with $B^{-1}(C')$: $y = -1/x$, so is naturally partitioned as $\{I_1^2, I_2^2, I_3^2\}$. Hence under B, P_2K transforms to $P_0JK = I_1^3 \cup I_2^3 \cup I_3^3$ in figure 10d, passing first through J, then intersecting $x = -1$. Arc I_4^2 of figure 10c maps to a similar arc I_4^3 in figure 10d attracted towards the axes by the stable fixed points on the axes. Loop I_5^2 of figure 10c maps to a similar narrower loop on the other side of the y-axis on account of the stable orientation-reversing fixed points below J. Comparing figures 10a and 10d, we now see how repeatedly applying B extends the portion P_0J of $W^u(P_0)$ into the third quadrant. Under still more applications of B^3, the portion of $W^u(P_0)$ shown in figure 10d extends as follows: I_1^3 extends as just described; I_2^3 and I_4^3 each transform into a sequence of arcs connecting J and K, attracted onto the interval JOK of the axes by the fixed points there, while I_3^3 and I_5^3 transform into a sequence of loops based at K and J respectively. These alternate from one side of the axis to the other, and are attracted to short intervals of the negative x- and y-axes, respectively, by the fixed points there. This behaviour is partially illustrated in figure 9a and is verified by considering iterates under B of appropriately chosen regions containing the various arcs I_k^j. The corresponding parts of $W^u(P_1)$ and $W^u(P_2)$ are very similar in character, comprising initial parts P_1J and P_2K respectively, followed by a sequence of arcs connecting J and K together with sequences of loops based at J and K. These are also shown in figure 9.

The remainder of $W^u(P_0)$ is a curve extending to infinity in the fourth quadrant. An asymptotic analysis shows that $y \sim -x^\gamma$ where $\gamma = (\sqrt{5}-1)/2$, which is confirmed numerically. The corresponding parts of $W^u(P_1)$ and $W^u(P_2)$ are similar curves with an analogous asymptotic power law between $\pm y$ and $\pm x$, and are shown in figures 9b and c.

The stable manifold $W^s(P_0)$ can be similarly understood by applying B^{-1} to a portion of $W^s(P_0)$ near P_0. Part of $W^s(P_0)$ is shown in figure 9d. If, in figure 8a, the whole curve shown there is regarded as the initial part of $W^s(P_0)$, then figure 8d shows that application of $(B^{-1})^3$ replicates the curve exactly and generates the four loops adjacent to the axes. Further iteration by B^{-3} merely generates an infinite sequence of loops in a fashion similar to that described in §3. The stable manifolds of P_1 and P_2 are similar, comprising a curve asymptotic to $x = -1$ at one end, and the negative x-axis at the other, akin to such curves shown in figures 8c and 8b respectively, together with an infinite sequence of loops which approach intervals on the coordinate axes. These intervals are indicated in figure 9. There is precisely one on each axis, extending beyond the values x_3, x_3', y_3', y_3 along the positive and negative x- and y-axes respectively. Because $B(W^s(P_i)) = W^s(P_{i+1})$, each of these intervals of accumulation is a limit of the stable manifolds of all three points P_0, P_1 and P_2; and for the same reason as given in §2, $y_3' = x_3$ and $x_3' = y_3$. These values are $x_3 = 5.0921423$ and $y_3 = -3.3819719$ to seven decimal places.

Knowledge of the structure of $W^s(P_i)$ now enables completion of the discussion of the behaviour under iteration by B^{-1} of the singular curves C and C', commenced in §3. Figure 10a shows the intersection of $B^{-1}(C'): y = -1/x$ and $B^{-1}(C): y = -1/x(x+1)$ with $W^u(P_0)$. Under iteration by B^{-3}, owing to the hyperbolic nature of P_0, points on these curves near P_0 are attracted towards P_0 along $W^u(P_0)$ and repelled along $W^s(P_0)$ (the arrows in figures 9 and 10 being reversed for this iteration). There is thus a general tendency of iterates under B^{-3} of these curves to increasingly resemble $W^s(P_0)$. In more detail, let us consider, for example, iteration under B^{-3} of the infinite arc $B^{-1}(C')$ shown in figure 10a, which we will temporarily call A_0. From

PHILOSOPHICAL TRANSACTIONS OF THE ROYAL SOCIETY A MATHEMATICAL, PHYSICAL & ENGINEERING SCIENCES

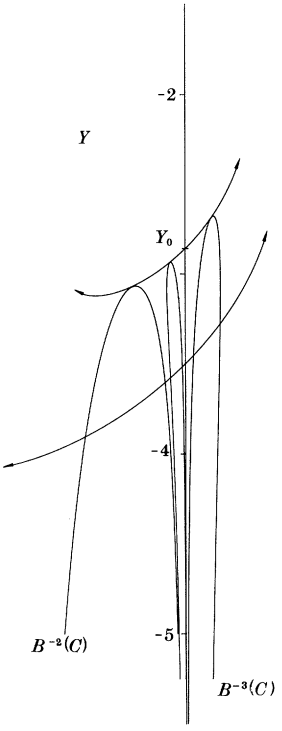

Figure 11. Bifurcation of unstable manifolds $W^{u}(Y)$ at $Y = Y_0$: for Y above Y_0 no intersection of $W^{u}(Y)$ with C or its preimages occurs; for Y below Y_0, transversal intersection of $W^{u}(Y)$ with C and all its preimages occurs.

figure 8, we recall that $B^{-3}(A_0)$ consists of another infinite arc A_1, nearer $W^{s}(P_0)$ than A_0, and the set of four loops $L_{1,0}$ lying close to the axes, shown in figure 8*d*. Under a further iteration by B^{-3}, the arc A_1 generates another arc A_2, closer to $W^{s}(P_0)$, and a set of four new loops $L_{2,0}$ closer than $L_{1,0}$ to the outermost loops of $W^{s}(P_0)$, shown in figure 9*d*. Similarly, in general, there is a sequence of arcs A_n approaching $W^{s}(P_0)$ such that $B^{-3}(A_n)$ comprises the next arc A_{n+1} and a set of four new loops $L_{n+1,0}$ lying closer to the outermost loops of $W^{s}(P_0)$ than $L_{n,0}$. Additionally, for each $n \geqslant 0$, the set of loops $L_{n+1,0}$ generated by A_n under B^{-3} has its own 'independent' future under further iteration: it forms a sequence of sets of loops $L_{n+1,m}, m = 1, 2, 3, \ldots$, where $L_{n+1,m+1} = B^{-3}(L_{n+1,m})$. These do not get closer to the outermost loops of $W^{s}(P_0)$, but are merely attracted to semi-infinite intervals I_{n+1} on the axes by the attractive nature of the fixed points there. As $n \to \infty$, the intervals I_{n+1} approach the corresponding limiting intervals of $W^{s}(P_0)$ shown in figure 9*f*. The behaviour for $y = -1/x(x+1)$ is similar. If iteration under B^{-1} is considered, there is an analogous accumulation onto $W^{s}(P_1)$ and $W^{s}(P_2)$ as well.

5. Unstable manifolds of fixed points on the *y*-axis

Knowledge of the behaviour of the preimages of the singular curves C and C' and also of the invariant manifolds of the period 3 points now enables description of the unstable manifolds of unstable fixed points on the y axis. Initially points below $y = -2$ are considered. All the phenomena described at the end of §2 will subsequently be explained.

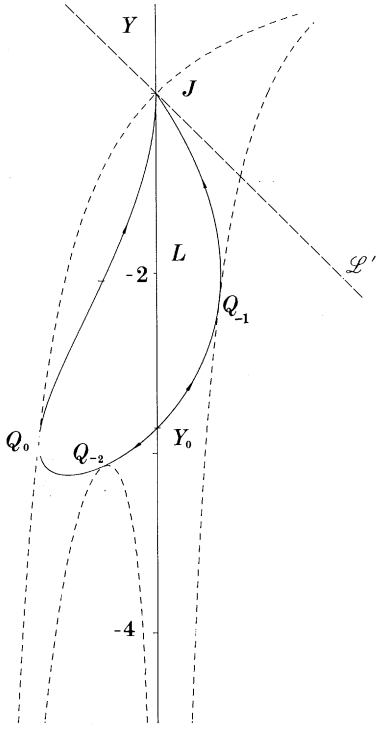

Figure 12. Tangential contact of $W^{\mathrm{u}}(Y_0)$ successively with $B^{-2}(C)$, $B^{-1}(C)$ and C at Q_{-2}, Q_{-1}, Q_0 respectively, before passage through J.

5.1. *Unstable manifolds in a neighbourhood of* $(0, -2)$

Consider initially the point $Y_0 : (0, y_0)$, shown in figure 6, representing the highest point on the y-axis of all the intervals of accumulation of the preimages of the singular curves C and C'. We recall that this process of accumulation arises from iteration under B^{-1} in which points near the negative y-axis for $y < -2$ are attracted towards that axis along the B-unstable manifolds of fixed points on the axis. The attraction of the loops is illustrated in figure 11 (where the arrows should be read backwards). It is clear from this figure that a fixed point $(0, y)$ with $y = y_{0+}$ has an unstable manifold, meeting none of these loops, whereas if $y = y_{0-}$, the unstable manifold meets all of these loops. The fixed point $Y_0 : (0, y_0)$ is the dividing case and its unstable manifold meets all the loops and their iterates under B tangentially. Now these loops are preimages of the curve $C : y = -1/(x+1)$, so that $W^{\mathrm{u}}(Y_0)$ eventually makes tangential contact with $B^{-2}(C), B^{-1}(C), C$ before passing through the point $J = (0, -1)$. This is illustrated by the results of numerical calculation in figure 12, where the contact points with these three curves can be obtained as follows. Consider the portion $Y_0 Q_{-2}$. Under B, this maps onto $Y_0 Q_{-1}$ (recall that B is locally orientation-reversing along $W^{\mathrm{u}}(Y_0)$), which in turn maps to $Y_0 Q_{-2} Q_0$. Now Q_0 lies on C, which is mapped in entirety onto the point J by B, so that the next image is $Y_0 Q_{-1} J$. J is a fixed point, and it is easily shown that the image of a line element at J is another line element at J tangential to the y-axis. Thus the image of $Y_0 Q_{-1} J$ is $Y_0 Q_{-2} Q_0 J$ which runs 'vertically' into J. The image of $Y_0 Q_{-2} Q_0 J$ introduces a new feature: the portion $Y_0 Q_{-2} Q_0$ has already been dealt with above, yielding $Y_0 Q_{-1} J$; but for the

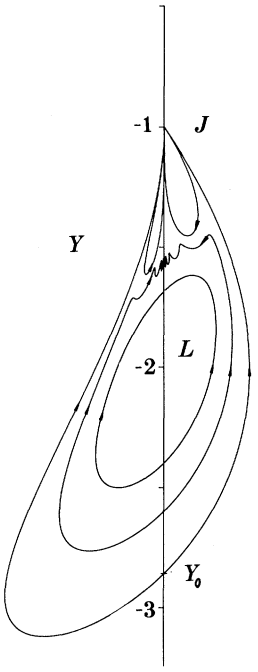

Figure 13. Initial parts of $W^u(Y_0)$ including the first two of the infinite sequence of loops based at J. Also shown are invariant manifolds $W^u(Y)$ for Y between L and Y_0 showing the development of oscillatory behaviour as Y approaches Y_0.

portion $Q_0 J$, since both end points Q_0 and J map to J, we deduce that a loop based at J must be formed. It may be shown that a line element l meeting C has an image $B(l)$, which is a line element at J whose direction depends only upon the location of l along C. Thus the loop $B(Q_0 J)$ emanates from J tangentially to $Y_0 Q_{-1} J$ and reapproaches J tangential to the y-axis. Further iteration merely produces more loops based at J, alternating from one side of the y-axis to the other, tending towards an interval of the y-axis below J (due to attraction of the fixed points there). Numerical confirmation of this is shown in figure 13.

Also shown in this figure are the unstable manifolds of two fixed points on the y-axis between $L:(0,-2)$ and Y_0. From §2, it is known that for $y=-2_-$, these form approximately nested invariant closed curves (figure 2*g*). None of the unstable manifolds emanating between L and Y_0 pass through J, and all of them must remain within the region bounded by the invariant curve $W^u(Y_0)$. We conjecture that these manifolds foliate this region: we can show that if polar coordinates (r,θ) with origin at L are used, then for all points with sufficiently small $r>0$, under the mapping B^2, θ increases when $-\frac{1}{2}\pi<\theta<\frac{1}{2}\pi$ and decreases when $-\frac{3}{2}\pi<\theta<-\frac{1}{2}\pi$. This is consistent with the motion shown on the approximate ellipses in figure 2*g*. Additionally, we have seen that, under B^2, points on $W^u(Y_0)$ move monotonely along $W^u(Y_0)$ from Y_0 to J. Consider now a straight line segment l extending from L to a point on $W^u(Y_0)$. By iterating backwards under B^2, the segment l maps into a sequence of arcs between L and $W^u(Y_0)$, which, the above considerations suggest, tends towards the straight line segment LY_0. But every fixed point Y between L and Y_0 has a unique local unstable manifold emanating at 45° with the y-axis. Thus for any such Y, ultimately some arc meets $W^u(Y)$ transversely. Now by iterating forward

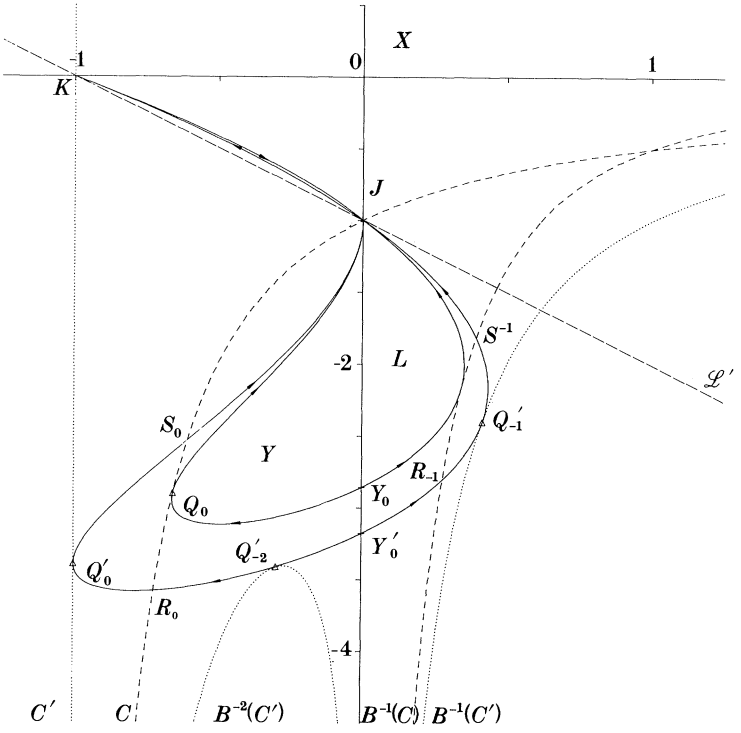

Figure 14. The initial parts of $W^u(Y'_0)$, showing the first loop JKJ which smoothly extends the arc $Y'_0 Q'_{-1} J$, and of $W^u(Y_0)$ as far as the point J.

under B^2, it follows that l meets transversely the unstable manifolds $W^u(Y)$ of all points Y strictly between Y_0 and L. Numerical evidence supporting this conclusion is shown in figure 13. By continuity, the unstable manifold $W^u(Y)$ of a point Y, approaching Y_0 from above, must be close to $W^u(Y_0)$. Thus such manifolds develop oscillations near and below J as they negotiate the bays between successive loops of $W^u(Y_0)$ based at J. An explanation of the first phenomenon mentioned at the end of §2 and illustrated in figure 3*a* is thereby given.

5.2. *Unstable manifolds emanating from fixed points between Y_0 and Y'_0*

We are now able to deduce the behaviour of unstable manifolds $W^u(Y)$ for points Y between Y_0 and Y'_0, where $Y'_0 = (0, y'_0)$ is the uppermost point of all the intervals of accumulation of the loops $B^{-2}(C'), B^{-3}(C'), B^{-4}(C'), \ldots$. The unstable manifold $W^u(Y'_0)$ starts out in a fashion similar to that shown in figure 11 and separates those manifolds which do not meet C' and its preimages from those which do. Its further development resembles that of $W^u(Y_0)$ and is sketched in figure 14. Under two iterations by B, $Y'_0 Q'_{-2}$ maps initially to $Y'_0 R_{-1} Q'_{-1}$, then to $Y'_0 Q'_{-2} R_0 Q'_0$. Consider $Y'_0 Q'_{-2} R_0$. Because $R_0 \in C$, and B maps all of C to the point J, the image of $Y'_0 Q'_{-2} R_0$ is $Y'_0 R_{-1} Q'_{-1} S_{-1} J$. The latter cannot meet the line $\mathscr{L}' : x + y = -1$ before J: the preimage of any such meeting point would be unbounded. The image of $Y'_0 R_{-1} Q'_{-1} S_{-1} J$, in turn, is $Y'_0 Q'_{-2} R_0 Q'_0 S_0 J$. Partition this as $\{Y'_0 Q'_{-2} R_0, R_0 Q'_0 S_0, S_0 J\}$. The image of the first of these has just been considered. $R_0 Q'_0 S_0$ is an arc with end-points on C and an interior point meeting C'. Thus its image is the pair of arcs

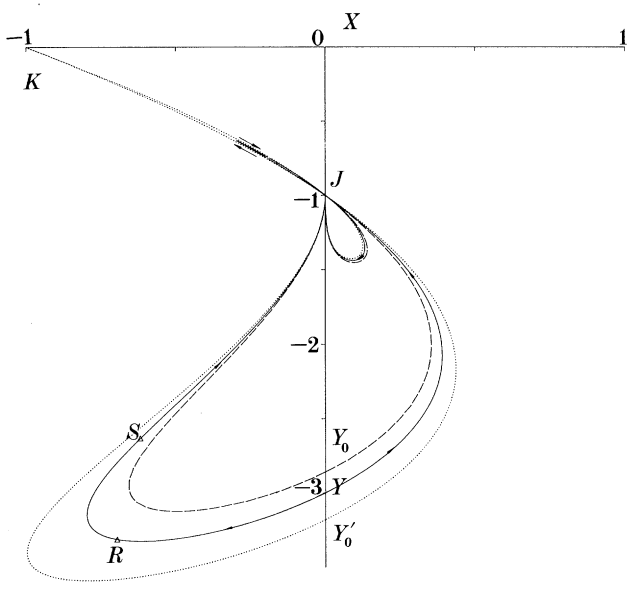

Figure 15. As figure 14, but now also showing the first loop based at J of $W^{u}(Y_0)$ (broken curve), containing within it the corresponding loop of $W^{u}(Y_0')$ (dotted curve). Between $W^{u}(Y_0)$ and $W^{u}(Y_0')$ lies $W^{u}(Y)$ described in §5.2 of the text.

JKJ. A consideration of the image of the region bounded by C and C', and below $x = -1$ (see figure 29) shows that this pair of arcs JKJ lies between $\mathscr{L}'$ and the axes. The image of $S_0 J$ is a loop based at J, not shown in figure 14. This is similar to the corresponding loop $B(Q_0 J)$ shown in figure 13. Recalling that under B, the location of a point on C determines a *direction* associated with its image at J, we can show that the loop $B(S_0 J)$ must emanate from J less steeply inclined to the negative y-axis than the loop $B(Q_0 J)$. In consequence, the loop $B(S_0 J)$ lies wholly within the loop $B(Q_0 J)$ except at J itself. By iterating these portions of $W^{u}(Y_0')$ still further, the two arcs connecting Y_0' and J behave in a fashion already described, the pair of arcs JKJ generate more arcs JKJ which are attracted onto the interval KOJ of the axes by the fixed points there, and the loop based at J generates further loops based at J similar to and lying within the corresponding loops for $W^{u}(Y_0)$. Because B is smooth at R_0 and S_0, the unstable manifold $W^{u}(Y_0')$ passes smoothly through J. Further, pairs of arcs JKJ meet tangentially at K for similar reasons to the tangencies in $W^{u}(Y_0)$ at J. This appearance is illustrated in figure 15, where the unstable manifold $W^{u}(Y)$ for Y between Y_0 and Y_0' is also shown. This manifold is trapped between $W^{u}(Y_0)$ and $W^{u}(Y_0')$, so has initial portions extending up to J. Referring also to figure 14, we see that the portion YJ of $W^{u}(Y)$ in the third quadrant must cut C at R (say) between R_0 and Q_0, and again at S (say) between Q_0 and S_0, but it does not meet C'. This arc RS between arcs $R_0 Q_0 S_0$ and $R_0 Q_0' S_0$ of figure 14 has both endpoints on C, and thus maps to the loop inside JKJ of figure 15. The arc SJ in figure 15 lies between $Q_0 J$ and $S_0 J$ of figure 14. Now the images of $Q_0 J$ and $S_0 J$ are the innermost and outermost 'small' loops based at J in the fourth quadrant in figure 15. Thus the image of SJ is itself a loop based at J between the two just mentioned. Under further iteration by B, the loops based at J are attracted to the axes by the fixed points there. Those below J alternate from one side of the axis to the other, but those above tend

inwards from the left only. Thus $W^u(Y)$ appears as in figure 3*b*, the suffices labelling each interval increasing with each pass through J, and the intervals related by $I_n = B(J_n)$. This explains the second property mentioned at the end of §2.

5.3. *Unstable manifolds emanating from fixed points between Y_0' and Y_3*

As we proceed further down the y-axis, the next important bifurcation point in the behaviour of the unstable manifolds is $Y_3 : (0, y_3)$. This is the endpoint of the interval of accumulation of the loops of the stable manifolds of the period 3 points P_0, P_1, P_2 (see figure 9*d–f*). The principal features of its unstable manifold are illustrated in figure 16, although the arcs and loops shown there do not form a continuous sequence along $W^u(Y_3)$. A detailed theoretical description of the build-up of this overall shape, which does use a continuous sequence along $W^u(Y_3)$, now follows in connection with figure 17. In figure 17*a* are shown the arcs I_0 and I_1 extending from Y_3 to J. These are wholly analogous to $W^u(Y_0)$ (shown in figure 12), and make corresponding tangential contacts with $W^s(P_0)$ and $W^s(P_1)$, as illustrated. The arc I_1 cuts the singular curve C twice. Let the first intersection be at R_3. Then $B(Y_3 R_3) = I_0$, and as $R_3 J$ is the smooth extension of $Y_3 R_3$, it follows that $B(R_3 J)$ gives the smooth extension of I_0 along $W^u(Y_3)$ through J. Further, because $B(I_0) = I_1$, it follows that along I_1, the point J is the image under B^2 of R_3. Thus each time B^2 is applied successively to $R_3 J$, a new portion of $W^u(Y_3)$ is generated, joining smoothly to the previous portion. The arc $R_3 J$ is partitioned naturally into four parts, divided by its intersections with the singular curves C and C'. As we progress along $W^u(Y_3)$ from R_3, the images of these parts are successively, I_2, I_3, I_4, I_5 shown in figure 17*b* (with I_2 smoothly extending I_0). Explanation of the arcs I_2, I_4 and the loop I_5 is similar to previous cases and needs no further discussion. The loop I_3 is the image of the part of $R_3 J$ to the left of C' (figure 17*a*). Because this part has end points on C' and touches $W^s(P_1)$ in the third quadrant, its image, I_3, has endpoints at K and must touch $W^s(P_2)$ in the second quadrant. Under a further iteration, the arcs I_2, I_4 and the loop I_5 map to I_2^1, I_4^1 and I_5^1 respectively, shown in figure 17*c*, and needing no discussion. The loop I_3 lies close to $W^u(P_2)$, whose behaviour under the mapping is shown in figure 10*c*, *d*. Like $W^u(P_2)$, I_3 cuts the curves $B^{-1}(C') : y = -1/x$ and $C : y = -1/(x+1)$ and thus $B(I_3)$ is the loop $I_{31}^1 \cup I_{32}^1 \cup \ldots \cup I_{35}^1$ based at K, turning downwards into the third quadrant, cutting $x = -1$, passing through J, and extending in a loop to $W^s(P_0)$ before returning via J back to K. This entire section of manifold is described in the order $I_2^1, I_{31}^1, \ldots,$ I_{35}^1, I_4^1, I_5^1 and joins smoothly onto I_1. The result of a further iteration is given in figure 17*d*: I_2^1, I_4^1, I_5^1 map to I_2^2, I_4^2, I_5^2 respectively: I_{31}^1 and I_{35}^1 have both endpoints on C' and thus have images I_{31}^2 and I_{35}^2 which are loops based at K; I_{32}^1 and I_{34}^1 extend from C' to J and thus map to arcs I_{32}^2, I_{34}^2 between K and J; I_{33}^1 is a loop based at J touching $W^s(P_0)$ and has image $I_{331}^2 \cup \ldots \cup I_{335}^2$ which is also a loop based at J extending to $W^s(P_1)$. This whole section of manifold is described in the order $I_2^2 I_{31}^2 I_{32}^2 I_{331}^2 \ldots$ $I_{335}^2 I_{34}^2 I_{35}^2 I_4^2 I_5^2$ and joins smoothly onto I_5. Lastly, considering one iterate of figure 17*d* in detail, we see (below) that the curve shown in figure 17*e* emerges. Because certain features of this are too fine to be readily discerned, a topological distortion of this figure to aid interpretation is provided in figure 17*f*. A partial confirmation of one of these distortions is provided by the inset of figure 17*e*: the apparently single loop below and to the right of J splits into two on enlargement, and this is incorporated into figure 17*f*. The disposition of the curve shown in figure 17*e* (or *f*) is now explained as follows. All the arcs connecting J and K map to similar arcs nearer the axes and the loops I_{31}^2, I_{35}^2 and I_5^2 map to similar narrower loops on the other side of

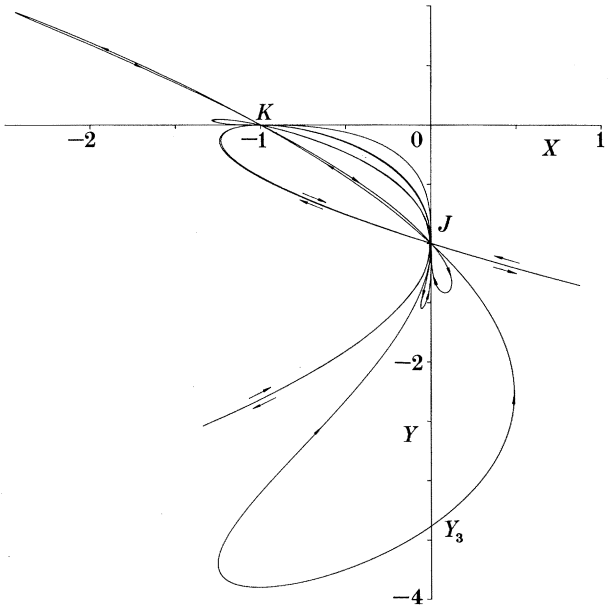

Figure 16. Initial portion of $W^u(Y_3)$, already showing the principal asymptotic features of the whole manifold which recur in infinite sequences: (i) arcs JK; (ii) small loops based at J and K; (iii) large loops based at J and K. See §5.3 of text.

the axis. The large loop $I^2_{331} \ldots I^2_{335}$ behaves as follows: I^2_{331} and I^2_{335} connect C to J and thus have images forming a nested pair of loops I^3_{331} and I^3_{335} based at J (see inset, figure 17*e*); I^2_{332} and I^2_{334} extend between C and C', so have images which are the arcs I^3_{332} and I^3_{334} between J and K; I^2_{333} has endpoints on C' and also touches $W^3(P_1)$, hence has as an image I^3_{333} in the form of a loop based at K, extending to $W^s(P_2)$.

The asymptotic behaviour now follows from figure 17 without difficulty. Comparison of figures 17*b* and 17*e* shows that under three iterations by B, the section of $W^u(Y_3)$ shown in figure 17*b* has virtually replicated itself, and additionally generated further arcs between J and K approaching the axes and further small loops based at J and K. Further iteration, therefore, merely produces, in addition to the union of all the curves in figures 17*a–e* infinite sequences of: (i) arcs JK tending to the interval JOK of the axes; (ii) small loops based at J and K tending to the axes, and (iii) large loops similar to I_3 based at K, and I^1_{33} & $I^2_{331} \cup \ldots \cup I^2_{335}$ based at J, making tangential contact with $W^s(P_2)$, $W^s(P_0)$ & $W^s(P_1)$ respectively and tending to the arcs KP_2, JP_0 and JP_1 of $W^u(P_2)$, $W^u(P_0)$, $W^u(P_1)$ respectively. In connection with (iii), recall the hyperbolic nature of the point P_2. Under B^3, points near P_2 are strongly attracted in the direction of $W^s(P_2)$ and strongly repelled along $W^u(P_2)$. Thus the loop I_3 only (in figure 17*b*) has an image under B^3 (figure 17*e*) consisting of a new loop I^3_{333}, which is closer to $W^u(P_2)$, and additionally, extra bits that virtually replicate the whole of figure 17*b*. Under further iteration by B^3, the new loop I^3_{333} behaves similarly except that its image lies closer to $W^u(P_2)$. We may thus conclude that $W^u(Y_3)$ tends with increasing distance along this manifold away from Y_3 towards those parts of $W^u(P_0) \cup W^u(P_1) \cup W^u(P_2)$ extending inwards from P_0, P_1, P_2 (see figure 10). The beginnings of this behaviour are manifest in figure 16. We also note, for use below, that we can regard the repetitive behaviour described above as being 'created' by these large loops I_3, I^1_{33} and $I^2_{331} \ldots I^2_{335}$ emanating from K and J.

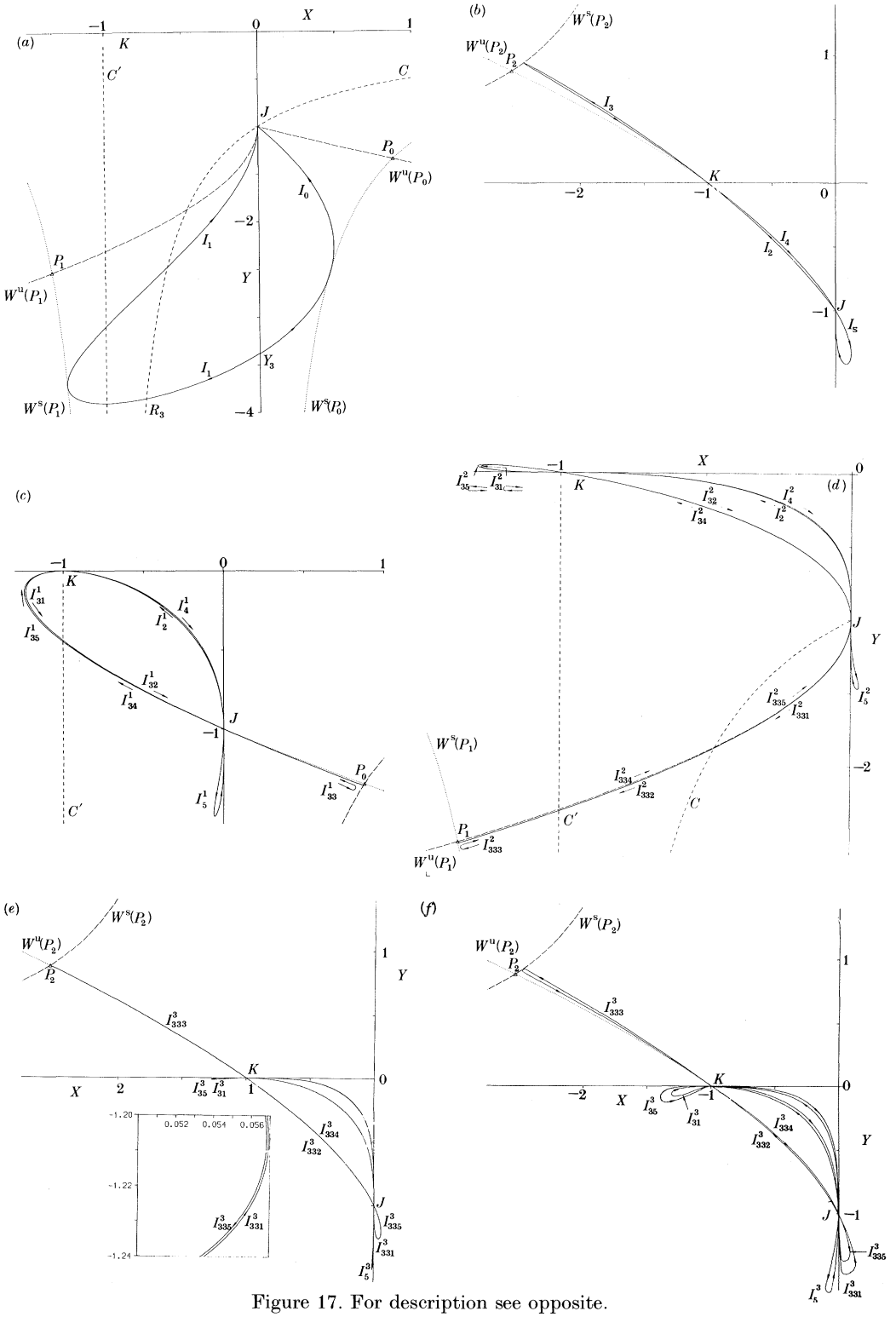

Figure 17. For description see opposite.

Behaviour of $W^u(Y)$ for points Y between Y_0' and Y_3 may now be described, again by using figure 17. $W^u(Y)$ starts with two arcs YJ similar to I_0 and I_1 of figure 17*a*. Because this part of $W^u(Y)$ lies between the corresponding parts of $W^u(Y_0')$ and $W^u(Y_3)$, the arc YJ in the third quadrant cuts C' twice, but does not meet $W^s(P_1)$. When B is applied a curve similar to figure 17*b* results, save only that the loop Λ based at K does not extend as far as $W^s(P_2)$. The general pattern of future behaviour is now similar for all the points Y considered, but the precise details depend crucially on the extent of the loop Λ. The next iterate of this whole section resembles figure 17*c*, the main difference being in the loop $B(\Lambda)$ extending from K. This is a truncated version of the loop $I^1_{31} \dots I^1_{35}$. If it stops short of J, the next iterate does not possess a loop analogous to $I^2_{331} \dots I^2_{335}$ and, following the interpretation at the end of the previous paragraph, further replication now effectively ceases. All that remains under further iteration is a sequence of arcs KJ and small loops based at J and K which tend towards the axes. If $B(\Lambda)$ does pass through J, then the next iterate does contain a shortened loop analogous to $I^2_{331} \dots I^2_{335}$. Ultimately, however, some iterate fails to contain a loop corresponding to the analogous loop of $W^u(Y_3)$. To see this, recall from the end of §4 that $W^s(P_2)$ is the limit of preimages of C and C'. Thus the loop Λ of $W^u(Y)$, similar to but shorter than I_3 in figure 17*b* cuts $B^{-3n}(C)$, but not $B^{-(3n+3)}(C)$ for some suitable $n \geqslant 1$. In consequence, while $B^{3n+1}(\Lambda)$ has a loop through J extending towards P_0, $B^{3n+4}(\Lambda)$ does not (see figure 17*c*). In summary, $W^u(Y)$ has an appearance somewhat like $W^u(Y_3)$, possessing in particular an infinite number of arcs JK and small loops which tend to the axes with iteration: but, whereas $W^u(Y_3)$ has infinitely many loops based at J and K, which extend towards P_0, P_1 and P_2, $W^u(Y)$ has only finitely many, which progressively shorten with iteration. This is the behaviour of (iii) at the end of §2 and is illustrated in figure 3*c*. Observe that the value of y for figure 3*c* does indeed lie between Y_0' and Y_3.

5.4. *Unstable manifolds emanating from fixed points below Y_3*

The final species of behaviour occurs for points Y below Y_3 and again can be understood theoretically by using figure 17. As before $W^u(Y)$ starts with two arcs YJ similar to the arcs I_0 and I_1 of figure 17*a*. Now, however, the arc YJ lies outside $W^u(Y_3)$ and so cuts $W^s(P_3)$ in two places (in a fashion similar to the way in which $W^u(Y_0')$ cuts C, illustrated in figure 14). Applying B yields a section of $W^u(Y)$ similar to that shown in figure 17*b*, but now the loop based at K extends beyond $W^s(P_2)$ into the second quadrant. If now B^3 is applied, this loop is attracted towards P_2 along $W^s(P_2)$ and simultaneously greatly extended into the second quadrant under the repulsion along $W^u(P_2)$. With still further applications of B^3, more loops are generated lying closer and closer to $W^u(P_2)$ and extending increasingly far along the unbounded branch of $W^u(P_2)$ in the second quadrant (see figure 10*c*). Similar increasingly long narrow loops tending towards $W^u(P_0)$ and $W^u(P_1)$ occur in the fourth and third quadrants. Other than this new feature, the remainder of this manifold behaves analogously to $W^u(Y_3)$. A manifold illustrating this behaviour is shown in figure 3*d*, and an explanation for the last point of §2 is now furnished.

Figure 17. Initial part of $W^u(Y_3)$ as far as J and four successive preimages showing the approximate self-replicating property of the curve, (*b*) and (*e*), required to elucidate the asymptotic behaviour of the manifold.

PHILOSOPHICAL TRANSACTIONS OF THE ROYAL SOCIETY A MATHEMATICAL, PHYSICAL & ENGINEERING SCIENCES

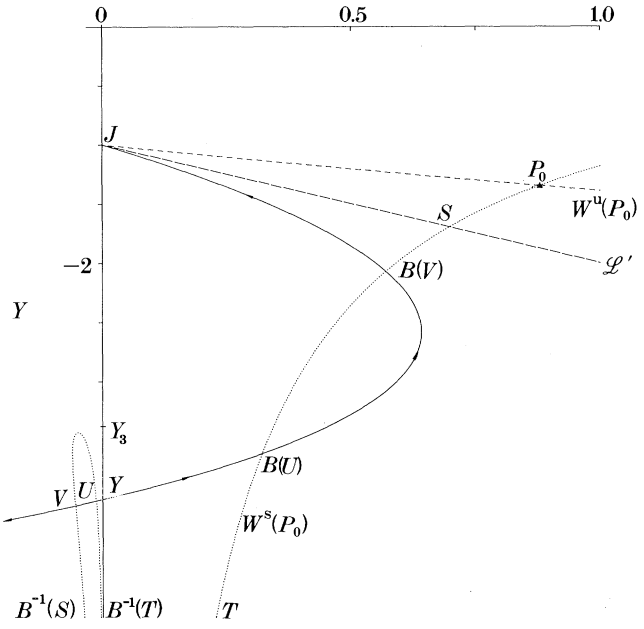

Figure 18. The first part of $W^u(Y)$ (solid curve) for Y below Y_3 and its intersections with part of $W^s(P_0)$ (dotted curve), used to determine the foliated region occupied by the first part of all manifolds with Y below Y_0.

5.5. *Regions foliated by manifolds $W^u(Y)$ when Y is below Y_0*

In preparing to answer the question of the overall foliation of the plane into invariant manifolds, we start to examine the region occupied by all the manifolds discussed so far. The primary technique used in describing a manifold $W^u(Y)$ has been to determine its appearance between Y and its first return to the y-axis, e.g. the intervals I_0 and I_1 of figure 17*a*: the rest then followed by iteration. Thus now, using theoretical considerations, we determine the whole region R filled out by the first part of all these manifolds, and the regions occupied by later parts of the manifolds may correspondingly be found by constructing the iterates of R. Figure 13 illustrates the conclusion that the unstable manifolds $W^u(Y)$ for Y between L and Y_0 are nested loops. For Y below Y_0, the first portions of $W^u(Y)$ must extend up to J (as I_0 and I_1 in figure 17*a*), and cannot intersect one another off the y-axis. So again they form a set of nested loops external to the corresponding loop JY_0J of $W^u(Y_0)$ in the nature illustrated in figure 19. In order to examine the full extent of the region occupied by these loops, we need to study the arcs YJ on $W^u(Y)$ for points Y far down the negative y-axis. Consider figure 18, in which is shown part of $W^s(P_0)$ (see figure 9*d*), in particular, its intersection at S with the line $\mathscr{L}'$ (mapped to infinity by B^{-1}) and T representing unboundedly large negative y values on the same branch of $W^s(P_0)$. The preimage $B^{-1}(ST)$ of the arc ST is the loop of $W^s(P_0)$ illustrated (shown dotted, and whose construction is explained in figure 8), and it should be recalled that there is an infinite collection of further preimages accumulating on the intervel below Y_3. The manifold $W^u(Y)$, for a point Y below Y_3, cuts these loops and so eventually cuts $B^{-1}(ST)$ in the points U and V as in figure 18. Hence it cuts ST at points $B(U)$ and $B(V)$. Now let $Y \to -\infty$. Then $W^u(Y)$ moves downwards so that $U \to B^{-1}(T)$ and $V \to B^{-1}(S)$. Hence $B(U) \to T$ while $B(V) \to S$. $B(V)$ cannot cross through S, otherwise

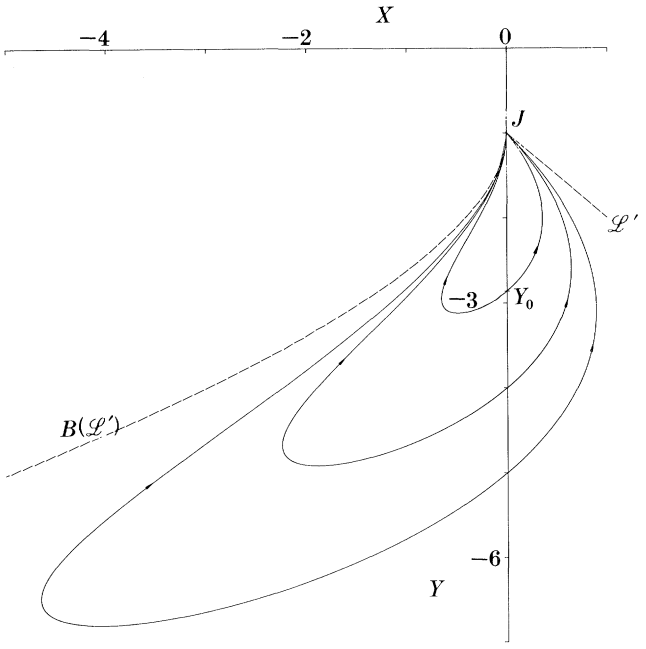

Figure 19. The region occupied by the first parts of manifolds $W^u(Y)$ with Y below Y_0, bounded by $W^u(Y_0)$, $\mathscr{L}'$ and $B(\mathscr{L}')$. Typical first parts of manifolds $W^u(Y)$ for $Y = (0, -4)$ and $Y = (0, -5)$ are also shown.

$B(UV)$ would intersect $\mathscr{L}'$ and the manifold would have to tend to infinity between U and V (and between all their preimages), and this does not happen. So the manifolds $W^u(Y)$ must have points which tend to S from below. Furthermore, if we consider the preimage under B of the line $y+x+1 = -\epsilon$, ϵ small and positive, just below $\mathscr{L}'$, we get a curve C'_ϵ just to the right of $C' : x = -1$. All the unstable manifolds $W^u(Y)$, restricted to the third quadrant, for Y under consideration cut the curve C'_ϵ (since they cut all the loops in the preimage of C' near the negative y-axis), and therefore have images lying close to $\mathscr{L}'$ in the fourth quadrant. We thus conclude that the whole region in the fourth quadrant exterior to $W^u(Y_0)$, between the negative y-axis and $\mathscr{L}'$, is foliated into a family of curves emanating from the y-axis and ultimately passing through J. Applying B, we obtain the corresponding foliated region in the third quadrant. This is exterior to $W^u(Y_0)$, bounded by the negative y-axis and $B(\mathscr{L}')$, which is the parametrized curve $(-x(1+x)^2+x, -(1+x)^2), x \geqslant 0$. The union of these regions is shown in figure 19. (The interior of $W^u(Y_0)$ is shown in figure 13.)

5.6. *Invariant manifolds emanating from the positive y-axis*

Fixed points $Y : (0, y)$ with $y > 0$ have unstable manifolds whose behaviour differs in detail from the manifolds considered above. They may be deduced, however, by similar methods. As before, there are changes in behaviour as the point Y moves across an endpoint of an interval of accumulation of the preimages of the singular curves C and C'. We therefore examine the first of these on the positive y-axis, the point $Y'_1 : (0, y'_1)$, where $y'_1 = 2.3138984$, as shown in figure 7. Referring to figure 5*c*, the interval (y'_1, ∞) of the y-axis is the limit of preimages of the loop $\bar{R}\bar{\bar{K}}\bar{\bar{Q}}_b$. For reasons similar to those advanced in §5.1, the unstable manifold of Y'_1 must touch all

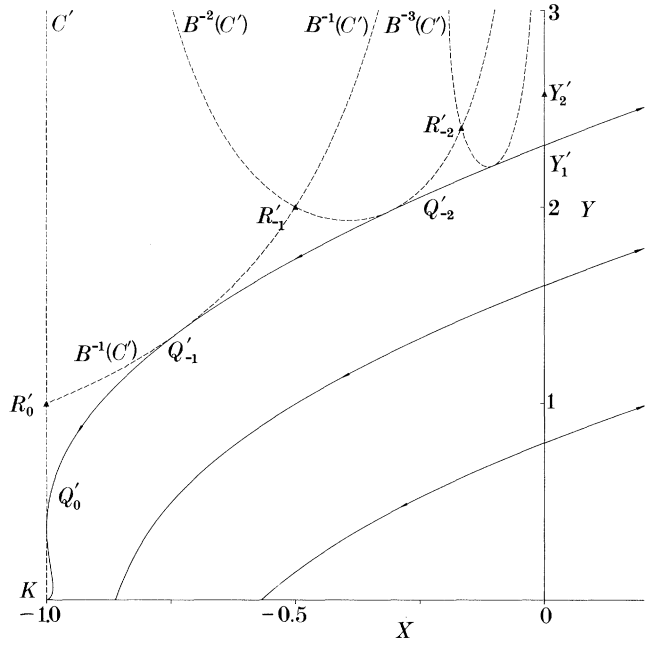

Figure 20. The unstable manifold of Y_1', where Y_1' is the lowest point of accumulation on the positive y-axis of the loops $B^{-n}(C')$, $n = 2, 3, \ldots$.

these loops tangentially in the second quadrant, and this is illustrated in figure 20. After the tangential contact with $B^{-1}(C'): xy = -1$ at Q_{-1}', there must be a similar contact with C' itself at Q_0' (since B is smooth at Q_{-1}'). Then, since the whole of C' is mapped to the point K, the arc $Q_{-1}' Q_0'$ is mapped by B to the arc $Q_0' K$ (the angle of approach at K depending on the y value of Q_0'). The image of the arc $Q_0' K$ is a loop based at K, hardly discernible in figure 20, but clearly visible in the inset of figure 21*a* as the broken loop based at K extending to the right of $x = -0.99$. Thereafter there is an infinite sequence of loops based at K, attracted to an interval of the x-axis. Points Y on the positive y-axis below Y_1' have unstable manifolds $W^{\mathrm{u}}(Y)$ whose restrictions to the second quadrant are bounded by the branch of $W^{\mathrm{u}}(Y_1')$, just described, and the axes which are invariant. As these unstable manifolds cannot cross or intersect, and sufficiently near the origin have been shown to behave as illustrated in figure 2*f*, we conjecture that all such manifolds emanate from the positive y-axis and accumulate on the negative x-axis between K and O. This conclusion is supported by numerical evidence (see figure 20). No loops are formed, but by continuity, the manifolds for Y near Y_1' have noticeable oscillations whilst approaching the x-axis as they negotiate the loops of $W^{\mathrm{u}}(Y_1')$ based at K (see figure 2*e* showing $W^{\mathrm{u}}(Y)$ for $Y = (0, 2.2)$, which lies close to Y_1'). From §2, there are similar oscillations in $W^{\mathrm{u}}(Y)$ for Y above but sufficiently near to O. In consequence, we conjecture that all the unstable manifolds $W^{\mathrm{u}}(Y)$ for Y between O and Y_1' exhibit these oscillations.

The behaviour described above is not unlike the behaviour in (say) the fourth quadrant of the manifolds $W^{\mathrm{u}}(Y)$ for Y between L and Y_0 as they approach the y-axis, shown in figure 13. But figure 20 also reveals a new feature: successive preimages $B^{-n}(C')$ and $B^{-n-1}(C')$ of the singular curve C' meet in the single point R_{-n}', where

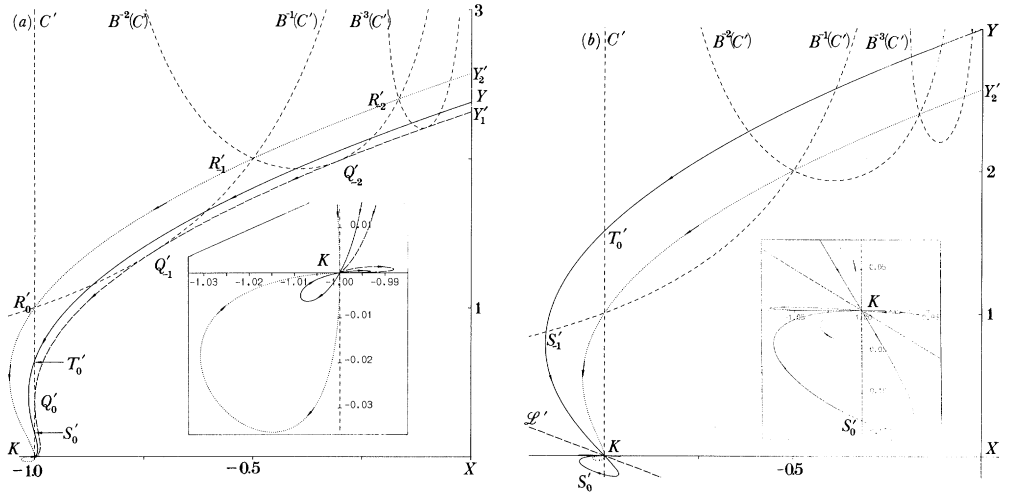

Figure 21. The unstable manifold within $x < 0$ of the point Y_2' (dotted curve), where Y_2' is the limit point of the sequence of points $\{R_{-n}'\}$, and R_{-n}' is the intersection point of the preimages $B^{-n}(C')$ and $B^{-n-1}(C')$ of the singular curve C'. Also shown are unstable manifolds $W^{\mathrm{u}}(Y)$ (solid curves) of points Y below and above Y_2'.

$R_0' = (-1, 1)$ is the unique point of intersection of $C' : x = -1$ with $B^{-1}(C') : y = -1/x$, and $R_{-n-1}' = B^{-1}(R_{-n}')$. The points R_{-n}', $n = 0, 1, 2, \ldots$, lying on $B^{-n}(C')$, must tend to the y-axis and do so at $Y_2' : (0, y_2')$, $y_2' = 2.5732688$, slightly above Y_1'. The point Y_2' is a further point in the bifurcation of unstable manifolds. The unstable manifold $W^{\mathrm{u}}(Y_2')$ passes through all the R_{-n}' (see figure 21*a*) and each arc $R_{-n+1}'R_{-n}'$ of $W^{\mathrm{u}}(Y_2')$ satisfies $R_{-n}'R_{-n+1}' = B(R_{-n-1}'R_{-n}')$. Finally, because $R_0' \in C'$, $B(R_{-1}'R_0') = R_0'K$, which lies wholly to the left of C'. An intersection of $W^{\mathrm{u}}(Y_2')$ with C' between R_0' and K would imply a corresponding intersection of $W^{\mathrm{u}}(Y_2')$ with $B^{-n}(C')$ between R_{-n+1}' and R_{-n}' for all $n \geqslant 1$. But for sufficiently large n, this cannot occur, because for such n, the loops of $B^{-n}(C')$ are extremely close to the y-axis and essentially vertical whereas $W^{\mathrm{u}}(Y_2')$ emanates from Y_2' at 45° to the axis. Thus for $n \geqslant 1$, $W^{\mathrm{u}}(Y_2')$ meets each loop of $B^{-n}(C')$ in precisely the two points R_{-n+1}' and R_{-n}'. Further iteration by B produces initially the larger loop based at K below the x-axis (shown dotted in figure 21), and thereafter, a sequence of loops based at K, not shown in the figure, accumulating on the x-axis follows due to the attraction of the fixed points there. A point Y between Y_1' and Y_2', as shown in figure 21*a*, has an unstable manifold (solid curve) between $W^{\mathrm{u}}(Y_1')$ and $W^{\mathrm{u}}(Y_2')$, so ultimately cuts C' in two points, S_0' and T_0'. By applying B, the arc $T_0'S_0'$ of $W^{\mathrm{u}}(Y)$ maps to the loop based at K inside the similar loop of $W^{\mathrm{u}}(Y_2')$, and then to a sequence of small loops approaching the x-axis, whereas the arc $S_0'K$ maps to the loop based at K inside the similar loop of $W^{\mathrm{u}}(Y_1')$, followed by similar asymptotic behaviour. This is illustrated in the inset of figure 21*a*. The behaviour of $W^{\mathrm{u}}(Y)$ for a point Y slightly above Y_2' is shown in figure 21*b*. Now as $W^{\mathrm{u}}(Y)$ is described, the first intersection with $B^{-n}(C')$ occurs before the last one with $B^{-n-1}(C')$. Thus, with $n = 0$, the arc $T_0'K$ of $W^{\mathrm{u}}(Y)$ cut off by C' has an interior point S_{-1}' where it meets $B^{-1}(C')$. In consequence, applying B to $T_0'S_{-1}'$, $W^{\mathrm{u}}(Y)$ extends smoothly beyond K into $\{x > -1, y < 0\}$ in a curve that must turn and cut C' at $S_0' = B(S_{-1}')$, and the image of $S_{-1}'K$ completes the return of this loop through S_0' to K. Under further iteration, each of the two arcs $S_0'K$ generates a sequence of loops based at K,

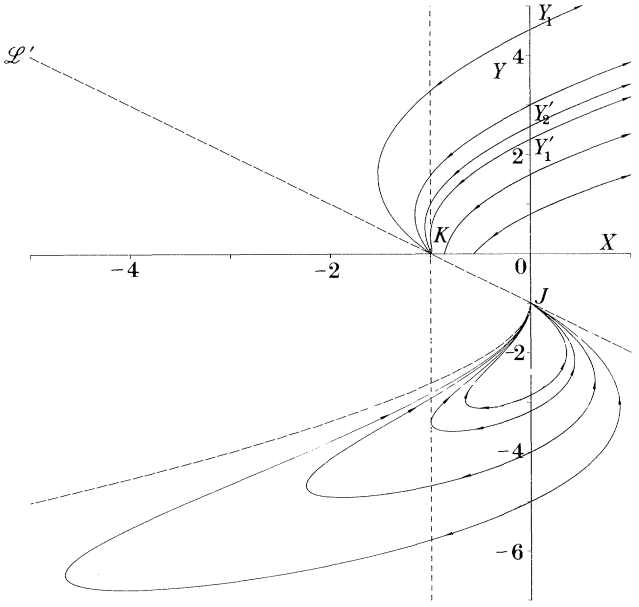

Figure 22. A summary of behaviour of partial manifolds in the 'fundamental region': the region in which the behaviour of the manifolds has been ascertained.

attracted to the x-axis, but whereas those in $x > -1$ approach from $y < 0$ only, those in $x < -1$ alternate across the x-axis. For points Y significantly higher up the y-axis, there are more transitions in behaviour as the point $Y_1 = (0, y_1), y_1 = 4.5240238$, the lowest accumulation point of the preimages of C (see figure 7), is traversed. Variations of behaviour akin to the changes for the fixed point Y_0' on the negative y-axis, already described, are now set in train. We do not attempt to describe these: instead of pursuing further the behaviour of individual unstable manifolds, we assemble those that we have described already and use them to obtain a global description of the foliation of the plane. To this end, we observe here that for all fixed points Y on the y-axis above Y_1', the arc YK of their unstable manifolds does not cross the line $\mathscr{L}'$. These arcs do, however, tend towards $\mathscr{L}'$ as Y moves up the y-axis. The reasons for this are the same as those leading to figure 19 and are to be found in §5.5 and the curves are illustrated in figure 22.

For completeness, we recall the behaviour for those parts of $W^{\mathrm{u}}(Y)$ for Y on the positive y-axis, which extend into the first quadrant. This was discussed in §2. It was shown there that the whole first quadrant is invariant, and that within it, motion is upward and to the right, so that invariant manifolds cannot accumulate on any invariant object. Thus the whole quadrant is foliated by manifolds. Further, the asymptotic analysis mentioned in §4 is applicable, and indicates that for $x, y \gg 1$, $y \sim x^{\gamma}$ where $\gamma = \frac{1}{2}(\sqrt{5}-1)$.

6. Global structure of the plane

In §5, the structure of significant parts of the plane was deduced theoretically, or at least strongly suggested by theoretical and numerical evidence. A summary of much of this, but which largely excludes asymptotic behaviour and the sequences of loops based at J and K, is provided by figure 22. Further behaviour follows, as before,

by iteration. Now the whole x-axis is composed of fixed points of B, and at a first glance, it appears that it is necessary to apply an analysis similar to that of §5 to such points. But we recall that $B = A^2$. So if W is the unstable manifold of $Y:(0, y)$ and thus satisfies $B(W) = W$, it follows that

$$B(A(W)) = A^3(W) = A(B(W)) = A(W):$$

that is $A(W)$ is also invariant under B. But $A(W)$ contains the point $A(0, y) = (y, 0)$, which is a fixed point on the x-axis, so that $A(W)$ is a B-invariant manifold of $(y, 0)$. Finally, because $DB(A(Y)) = DA(Y)\cdot DB(Y)\cdot DA^{-1}(Y)$, the eigenvalues of DB at $(y, 0)$ equal those of DB at $(0, y)$, and thus $A(W)$ must be the unstable manifold of $(y, 0)$. Thus, by merely applying A to $W^{\mathrm{u}}(0, y)$, we obtain $W^{\mathrm{u}}(y, 0)$. The same holds if A^{-1} is applied. Now in figure 22 only partial manifolds are shown, and in general, the images of these under A and A^{-1} are not the same. Hence, by a number of applications of A and A^{-1} to the partial manifolds shown in figure 22, we shall see below that we obtain a picture of the structure throughout the whole plane.

6.1. *The fundamental region and its image under A*

In the sequel, the region whose structure is known (figure 22) is regarded as a 'fundamental' region: all other regions are derived from it by application of A or A^{-1}. Furthermore, due to variations of behaviour across certain manifolds, as seen in §5, it is necessary to subdivide the fundamental region into various subregions.

The deduction of the qualitative shape of all the images of these various subregions and the structures of manifolds therein follows from purely theoretical considerations. We have chosen, however, to omit practically all the analytical details used to estimate the extent of these various images, as these calculations add little to our ultimate objective of describing the global structure of the plane. Instead, we have restricted ourselves to a descriptive treatment and, as far as possible, we have provided numerically generated pictures both to support and to illustrate the results presented. Certain phenomena described below such as sequences of loops (§6.3) or sequences of self-similar regions (§6.2) clearly cannot be illustrated numerically and are the result of deductive methods alone.

In figure 23*a*, the portion of the fundamental region lying in $y > 0$ is partitioned into regions $R_0, \ldots, R_{3a}$ and the images of these regions under A are also shown. Regions R_0 and $A(R_0)$, bordered by $W^{\mathrm{u}}(\mathrm{O})$ are self-explanatory. R_1 is the B-invariant region bounded by $W^{\mathrm{u}}(Y_1')$ and $A(R_1)$ is the B-invariant image region in $x > 0, y < 0$. R_2 is the region between $W^{\mathrm{u}}(Y_1')$ and $W^{\mathrm{u}}(Y_2')$ lying in the strip $-1 < x < 0$. Because A maps $C':x = -1$ to the point J, $A(R_2)$ is the wedge region X_1X_2J extending from the interval X_1X_2 of the positive x-axis towards the point J. Here $X_1 = A(Y_1')$ and $X_2 = A(Y_2')$. The angle at which X_2J approaches J is determined by where its pre-image, part of $W^{\mathrm{u}}(Y_2')$, intersects C'. This is the point $(-1, 1)$, namely R_0' in figure 21*a* and the discussion of §5.6, in consequence of which X_2J approaches J at 45° to the axes. The region R_{2a} is the narrow crescent region between $W^{\mathrm{u}}(Y_2')$ and C' (more clearly seen in figure 21). Under A, this forms the region $A(R_{2a})$, bounded by a loop based at J extending into the third quadrant. This loop, which is just discernible in the main figure, is clearly revealed by the blow-up of the neighbourhood of J. We shall see that this loop has a significant bearing on the structure of some of the invariant manifolds, in consequence of which, we shall refer to it below as the loop l. By smoothness of A at $(-1, 1)$, the upper part of the loop l is the extension of X_2J. So it also approaches J at 45° to the axes, while the part approaching J vertically is the image of $W^{\mathrm{u}}(Y_2')$

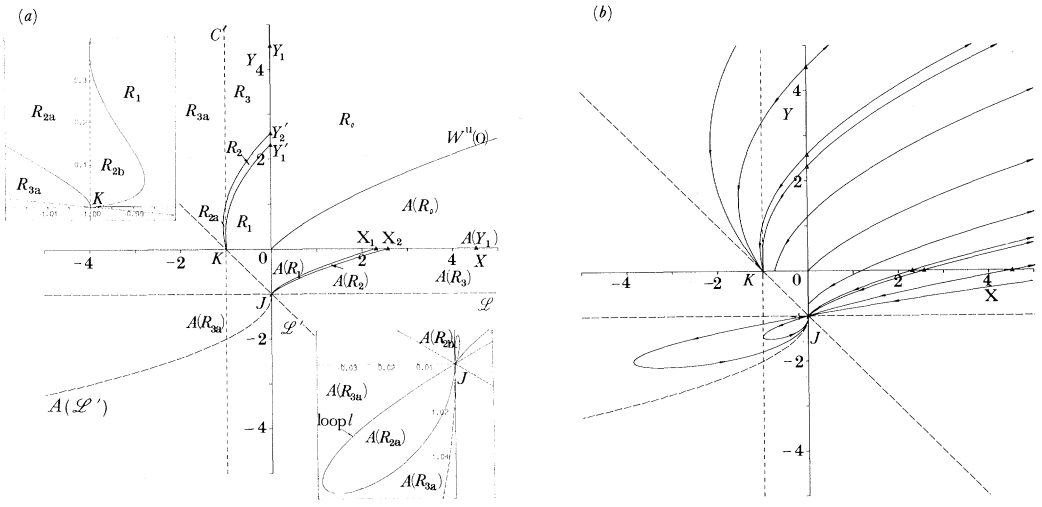

Figure 23. Partitioning of the fundamental region restricted to $y > 0$ into subregions $R_0, \ldots, R_{3a}$ and their images under A together with manifold structure within these subregions.

near K. For later use, we note that the loop l lies wholly below $C: y = -1/(x+1)$ in $-1 < x < 0$, and in consequence, l separates these loops based at J which cut C from those which do not. (If l met C other than at K, then applying A^{-1}, the curved boundary $R_0' K$ of R_{2a} (see figure 21*a*) would meet $A^{-1}(C) = B^{-1}(C'): y = -1/x$ at a point P (say) in addition to R_0'. This in turn would imply that $W^u(Y_2')$ meets $B^{-1}(C')$ in three points P, R_0' and R_{-1}'. But we showed in §5.6 that $W^u(Y_2')$ meets $B^{-1}(C')$ in precisely R_0' and R_{-1}' alone. Thus the loop l bounding $A(R_{2a})$ meets C at J only, and by considering how this loop approaches J, we see that it lies below C.) R_{2b} is the region adjacent to K between C' and the arc of $W^u(Y_1')$, as illustrated in the inset showing a blow-up of K. We saw in §5.6 that under iteration by B, this arc of $W^u(Y_1')$ generates an infinite sequence of loops of $W^u(Y_1')$ based at K, the first of which is clearly seen as the broken loop in the inset of figure 21*a*, and is responsible for the thickening of the x-axis near K in the inset of figure 23*a*. Denote by R_{2b}^* the union of R_{2b} with all regions enclosed by this sequence of loops (and observe that R_1 is exterior to all these loops). Then, under A, R_{2b} maps to a loop based at J, shown in the blow-up of J, and R_{2b}^* maps to an infinite sequence of loops based at J, accumulating on the y-axis. The region R_3 is the portion of the strip $-1 < x < 0$ above $W^u(Y_2')$ and has an image $A(R_3)$ comprising that part of the strip $-1 < y < 0$ to the right of $X_2 J$. The region R_{3a} is that part of the sector between C' and $\mathscr{L}'$ in the second quadrant exterior to R_{2a}, and has an image in the third quadrant bounded by the line $\mathscr{L}$, the loop l bounding $A(R_{2a})$ and the curve $A(\mathscr{L}'): x = -(1+y)^2$, $y < -1$. Observe that although R_3 and R_{3a} are adjacent regions, $A(R_3)$ and $A(R_{3a})$ have a common boundary point in J alone. This is because A is singular on C', mapping all of C' to J, while points near C' in R_3 are mapped to $y = -1+, x > 0$ and nearby points in R_{3a} are mapped to $y = -1_-, x < 0$.

The structure of the manifolds in the regions described above is shown in figure 23*b*. The region R_0 contains no singular curves of A, so its image is topologically equivalent to itself. R_1 behaves analogously. The other regions, however, all border onto C' and manifolds in these regions which cut C' are mapped to manifolds passing through J. In particular, the manifolds crossing R_2 and R_3 from the y-axis to C' all

become manifolds emanating from the x-axis focused into the point J, whereas the manifolds in R_{2a}, R_{2b} and R_{3a} all begin and end on C', so have images in the form of nested loops based at J. This is clearly shown in figure 23*b* for $A(R_{3a})$ but holds equally for $A(R_{2a})$ and $A(R_{2b})$. Also, following the argument of §5.6, we have inferred that the unstable manifolds $W^u(Y)$ in R_1 develop oscillations, indicative of heteroclinic behaviour, as they approach the negative x-axis. As heteroclinic behaviour is preserved under A, similar oscillations occur as the unstable manifolds $W^u(A(Y))$ in $A(R_1)$ approach the negative y-axis. This is consistent with the behaviour described in §2.

If further iteration by A is considered, $A(R_0)$ and $A(R_1)$ map to R_0 and R_1 respectively: thus $R_0 \cup A(R_0)$ and $R_1 \cup A(R_1)$ are A-invariant regions and nothing new is learnt by further iteration. To discuss R_2, reconsider figure 21*a*: R_2 is foliated by the beginnings of unstable manifolds $W^u(Y)$ extending from Y (between Y_1' and Y_2') to their first intersection with C'. Under application of B, such a portion of unstable manifold replicates itself and then extends onwards to K. Thus, in the notation of figure 23*a*, $B(R_2) = R_2 \cup R_{2a} \cup R_{2b}$, and because $B = A^2$, the second iterate of R_2 is known. Examination of further iterates therefore requires the behaviour of R_{2a} and R_{2b} under iteration. The future of R_{2b} lies in the loops $R_{2b}^* \cup A(R_{2b}^*)$ and is known. R_{2a}, however, yields initially the loop $A(R_{2a})$ and is then involved in a sequence of iterations, discussion of which we defer to §6.3. In a similar fashion, $A^2(R_3) = R_3 \cup R_{3a}$. The first iterate of R_{3a} is the region $A(R_{3a})$ exterior to $A(R_{2a})$, foliated by loops based at J and discussed earlier. Subsequent behaviour involves the period 3 points P_0, P_1, P_2 and is deduced immediately below.

6.2. *Self-similar behaviour near the period 3 points*

Consider now the state of play in the region below $\mathscr{L}: y = -1$. Following from figures 22 and 23*b*, our knowledge is summarized by figure 24. Within $W^u(Y_0)$, the internal structure of loops based at J (see figure 13) is still unknown, and in the third quadrant, behaviour in the sector S, bounded by the curves $A(\mathscr{L}')$ and $B(\mathscr{L}')$, is also to be found. We shall show a self-similar behaviour in S by keeping careful account of the iterates of boundaries of certain regions with known structure. To follow these boundaries, we introduce narrow semi-infinite strips bordering the singular line C' (the only singular curve of A) and we will refer to these strips and their images as 'neighbourhoods' of C' and its images, respectively. Thus, let neighbourhoods $\mathscr{N}_i, i = 1, 2, 3, 4$ be as illustrated in figure 25: they are neighbourhoods of C' in each of the four quadrants when K is regarded as origin. Some iterates of the $\mathscr{N}_i$ under A are also shown. The neighbourhoods $A(\mathscr{N}_i)$ are adjacent to $\mathscr{L}: y = -1$ and additionally are separated by the y-axis. This follows from $A(-1+\xi, \eta) = (\xi\eta, -1+\xi)$ and a consideration of the signs of ξ and η. The second iterates $A^2(\mathscr{N}_i)$, separated by $\mathscr{L}'$ and the x-axis follow similarly. Now $A^2(\mathscr{N}_1)$ and $\mathscr{N}_2$ border the region $R_{2a} \cup R_{3a}$ of figure 23*a*, so that $A(R_{2a} \cup R_{3a})$, the completely known region above the unknown sector S of figure 24, is bounded by $A(\mathscr{N}_2)$ and $A^3(\mathscr{N}_1)$ as shown in figure 25. The neighbourhood $A^3(\mathscr{N}_3)$, bordering S, immediately exterior to $A(R_{2a} \cup R_{3a})$ follows by continuity of A across $\mathscr{L}'$. From figure 24, the other region where the structure is largely known, is the region in the fourth and third quadrants below $\mathscr{L}'$ and $B(\mathscr{L}')$ respectively. In figure 25 this region is divided by the lines C' and the y-axis into subregions R_4, R_5 and R_6. Structure in R_4 is completely known (but in R_5 and R_6 loops at J need further examination). We recall from §5 that $R_4 \cup R_5 = B(R_6)$ and, in particular, the upper boundary of $R_4 \cup R_5$ is the image under B of $\mathscr{L}' \cap \{x > 0\}$, the

PHILOSOPHICAL TRANSACTIONS OF THE ROYAL SOCIETY A MATHEMATICAL, PHYSICAL & ENGINEERING SCIENCES

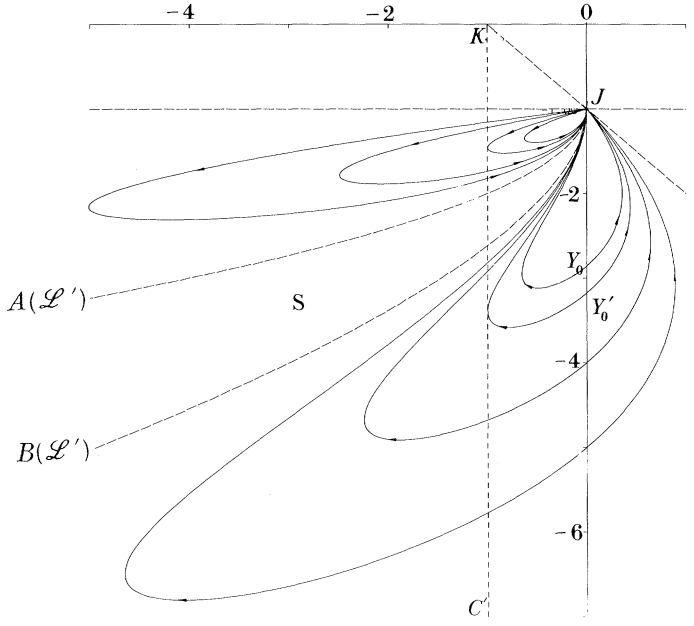

Figure 24. Summary of known manifold structure in the half-plane $y < -1$.

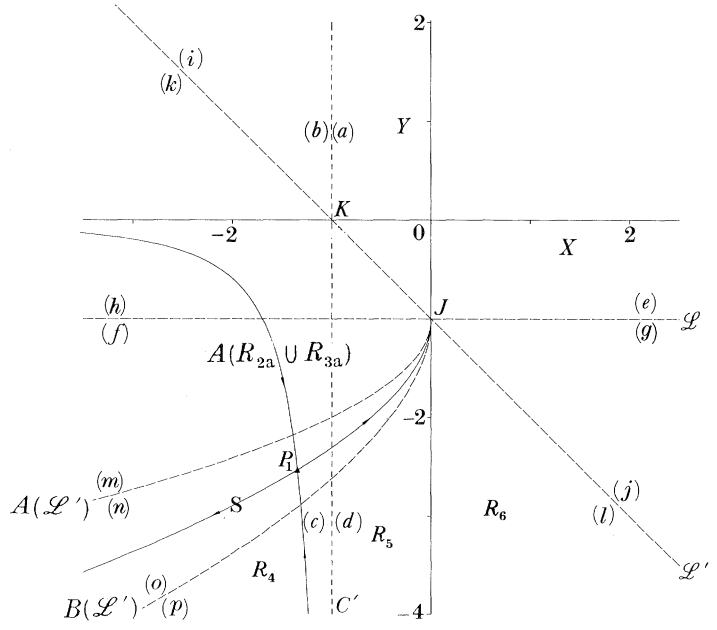

Figure 25. The strips $\mathscr{N}_1, \ldots, \mathscr{N}_4$ neighbouring C' and their iterates under several applications of the mapping A, employed to keep track of successive images of regions adjacent to the strip S (figure 26). (*a*) $\mathscr{N}_1$, (*b*) $\mathscr{N}_2$, (*c*) $\mathscr{N}_3$, (*d*) $\mathscr{N}_4$, (*e*) $A(\mathscr{N}_1)$, (*f*) $A(\mathscr{N}_2)$, (*g*) $A(\mathscr{N}_3)$, (*h*) $A(\mathscr{N}_4)$, (*i*) $A^2(\mathscr{N}_1)$, (*j*) $A^2(\mathscr{N}_2)$, (*k*) $A^2(\mathscr{N}_3)$, (*l*) $A^2(\mathscr{N}_4)$, (*m*) $A^3(\mathscr{N}_1)$, (*n*) $A^3(\mathscr{N}_3)$, (*o*) $A^4(\mathscr{N}_2)$, (*p*) $A^4(\mathscr{N}_4)$.

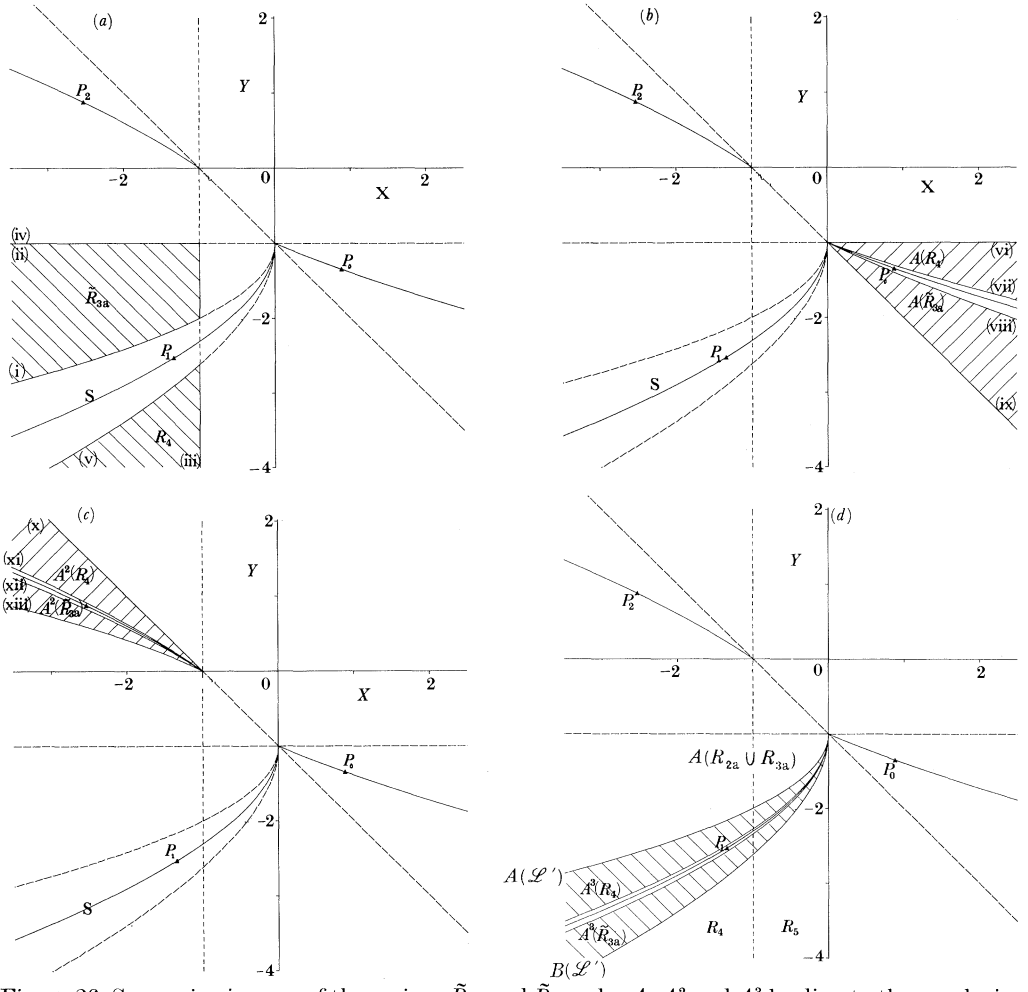

Figure 26. Successive images of the regions $\tilde{R}_{3a}$ and $\tilde{R}_4$ under A, A^2 and A^3 leading to the conclusion that S is divided into an infinite sequence of self-similar wedge-shaped regions accumulating onto $W^u(P_1)$. (i) $A^3(\mathscr{N}_1)$, (ii) $A(\mathscr{N}_2)$, (iii) $\mathscr{N}_3$, (iv) $A(\mathscr{N}_4)$, (v) $A^4(\mathscr{N}_4)$, (vi) $A(\mathscr{N}_3)$, (vii) $A^5(\mathscr{N}_4)$, (viii) $A^4(\mathscr{N}_1)$, (ix) $A^2(\mathscr{N}_2)$, (x) $A^3(\mathscr{N}_2)$, (xi) $A^6(\mathscr{N}_4)$, (xii) $A^5(\mathscr{N}_1)$, (xiii) $A^3(\mathscr{N}_2)$.

upper boundary of R_6. But $\mathscr{L}' \cap \{x > 0\}$ is bordered by $A^2(\mathscr{N}_2)$ and $A^2(\mathscr{N}_4)$, restricted to $x > 0$, so that $R_4 \cup R_5$ is bordered above by $A^4(\mathscr{N}_2)$ and $A^4(\mathscr{N}_4)$, restricted to $y < -1$. This is shown in figure 25 and it should be observed that we have thus shown that S is bordered by $A^3(\mathscr{N}_3)$ and $A^4(\mathscr{N}_2)$. The final ingredient necessary before we start iterating is the observation that P_1 lies in S along with a substantial part of its unstable manifold, while its stable manifold crosses transversely out of S, as shown. It can be established that the period three points of B are in fact period three points of A satisfying

$$P_{n-1} = A(P_n), \quad n = 0, 1, 2 \,(\mathrm{mod}\, 3)$$

and that attraction along the stable manifolds of the P_i occurs under A^3, but is now orientation-reversing.

Consider now iteration under A of regions R_4 and $\tilde{R}_{3a} = A(R_{3a} \cup R_{2a}) \cap \{x < -1\}$, which are shown hatched in figure 26*a*. Successive iterates of these regions are also

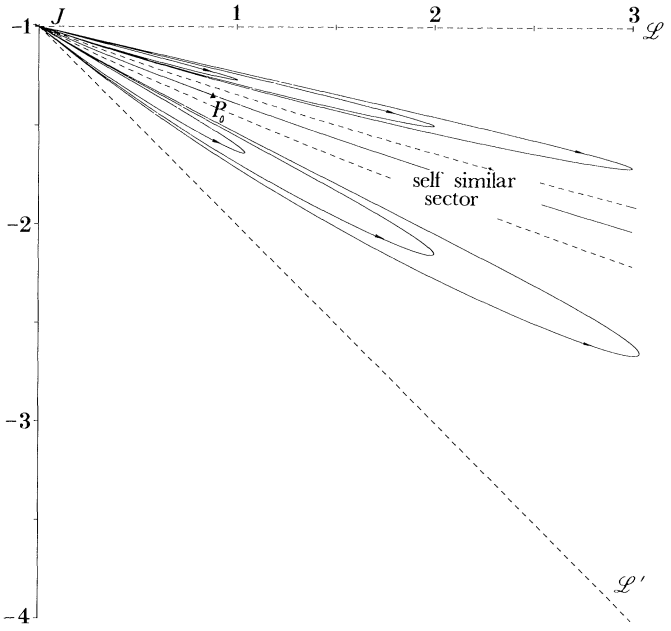

Figure 27. Representative loops of invariant manifolds in the outermost wedge regions of the self-similar sector which abutts $W^u(P_0)$.

shown hatched in the rest of figure 26. In figure 26*b*, $A(R_4)$ and $A(\tilde{R}_{3a})$ are shown. Because R_4 is bordered by $\mathscr{N}_3$, $A(R_4)$ is bordered by $A(\mathscr{N}_3)$, whose location was determined earlier. The other region bordering R_4, that is $A^4(\mathscr{N}_4)$, lies close to P_1 and so under A is attracted towards $P_0 = A(P_1)$. Thus $A(R_4)$ is the wedge-shaped region shown. The borders of $\tilde{R}_{3a}$ may be similarly followed: $A(\mathscr{N}_2)$ maps to $A^2(\mathscr{N}_2)$, described earlier in this section and shown in figure 25, the short interval of C' maps to J and $A^3(\mathscr{N}_1)$ maps to a region lying close to $W^u(P_0)$. We thus get another wedge-shaped region. Further iterates are shown in figures 26*c* and *d*. The essential point is that $A^3(R_4)$ and $A^3(\tilde{R}_{3a})$ are subsets of S each of which has a common boundary, namely $A(\mathscr{L}')$ and $B(\mathscr{L}')$ respectively with the original regions $A(R_{2a} \cup R_{3a})$ and $R_4 \cup R_5$ respectively lying adjacent to S. (This follows the observation made above that $A^3(\mathscr{N}_3) \subset A^3(R_4)$ and $A^4(\mathscr{N}_2) \cap \{y < -1\} \subset A^3(\tilde{R}_{3a})$ are borders for S). Thus if we repeat the process, i.e. restrict $A^3(R_4)$ and $A^3(\tilde{R}_{3a})$ to $x < -1$ and apply A^3 again, the attraction along $W^s(P_1)$ and repulsion along $W^u(P_1)$ yield further wedge-shaped regions within S extending to J, abutting $A^3(\tilde{R}_{3a})$ and $A^3(R_4)$ respectively. The whole of S is thus divided into an infinite sequence of wedge-shaped regions, which accumulate onto $W^u(P_1)$. There are similar sectors adjacent to $W^u(P_0)$ and $W^u(P_2)$ in the fourth and second quadrants respectively.

The structure in all these wedge-shaped regions is easily ascertained. Referring back to figure 24, we see that both $\tilde{R}_{3a}$ and R_4 are wholly composed of nested arcs beginning and ending on C'. These arcs all turn towards S, and thus towards $W^u(P_1)$ lying within S. Under iteration by A, all the endpoints on C' are mapped to J, so that $A(\tilde{R}_{3a})$ and $A(R_4)$ are foliated by nested loops based at J. A is non-singular throughout these regions and their images under A, so that the topological structures in $A(\tilde{R}_{3a})$, $A(R_4)$, $A^2(\tilde{R}_{3a})$, $A^2(R_4)$, $A^3(\tilde{R}_{3a})$ and $A^3(R_4)$ are all identical, consisting of nested loops. Considering the attractive nature of the points P_i, the loops in these

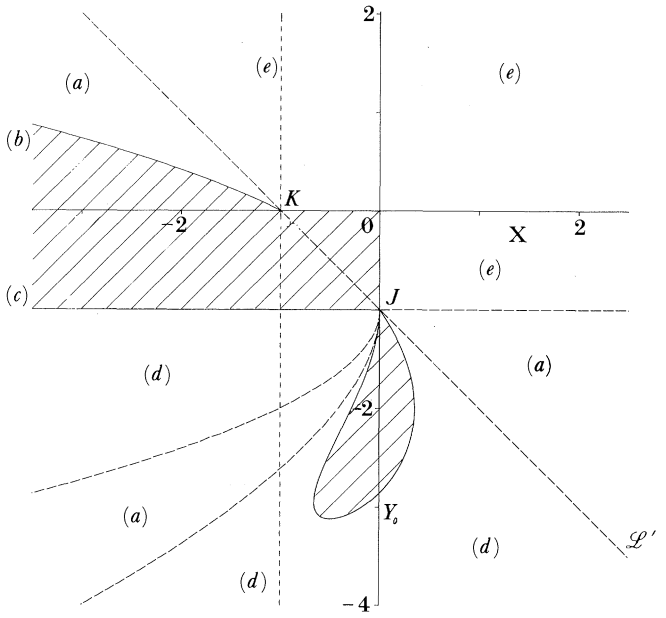

Figure 28. Outstanding regions of unknown structure (hatched), and references to regions of known structure. (*a*) Self-similar sector, (*b*) $A^3(\mathscr{N}_4)$, (*c*) $A(\mathscr{N}_4)$, (*d*) figure 24, (*e*) figure 23*b*.

various regions all turn towards the adjacent $W^{\mathrm{u}}(P_i)$. When this process is repeated, exactly the same structures recur: restricting $A^3(\tilde{R}_{3\mathrm{a}})$ and $A^3(R_4)$ to $x < -1$ replaces the nested loops based at J by nested arcs ending on C', and applying A transforms these to loops in the fourth quadrant based at J exactly as before. In summary, the sectors contain an infinite number of self-similar wedge-shaped regions foliated into nested loops based at J or K. The sector surrounding $W^{\mathrm{u}}(P_0)$ is illustrated in figure 27. Referring briefly back to figures 16, 17 and the associated discussion (§§5.3, 5.4), we can interpret these sectors as containing the totality of all the loops based at J and K that figured in that discussion. Now from the considerations immediately above, these loops lie on precisely those unstable manifolds which either enter R_4 or $\tilde{R}_{3\mathrm{a}}$ (figure 26*a*), and these unstable manifolds can be identified respectively as those emanating from points Y on the negative y-axis below Y_0' (see figure 22) and those on the positive y-axis above Y_1, defined in §3 and also shown in figure 22. The relevance of Y_1 is as follows: we recall from figure 23 and the discussion of §6.1 that all manifolds emanating into the second quadrant from points Y above Y_1' eventually enter $A(R_{2\mathrm{a}}) \cup A(R_{3\mathrm{a}})$ through J. But for a point Y very near Y_1', the subsequent excursion of the manifold $W^{\mathrm{u}}(Y)$ into $A(R_{2\mathrm{a}}) \cup A(R_{3\mathrm{a}})$ does not carry it as far as C'; and $\tilde{R}_{3\mathrm{a}}$ is that part of $A(R_{2\mathrm{a}}) \cup A(R_{3\mathrm{a}})$ to the left of C'. The point Y_1 has the property that $W^{\mathrm{u}}(Y_1)$ touches C' tangentially in $\tilde{R}_{3\mathrm{a}}$, and thus only points Y above Y_1 contribute to the loops based at J and K in the self-similar sectors.

6.3. *Internal structure of loops based at J meeting the y-axis tangentially*

In figure 28, we assemble all the regions whose structure is known with a brief description or reference to describe the structure. Two disconnected regions remain to be discussed. These are shown hatched. In the bounded region JY_0J, there remains to discuss the interior of the loops based at J (see figure 13), whereas virtually nothing is known about the other shaded region. Figure 29 gives a useful partitioning

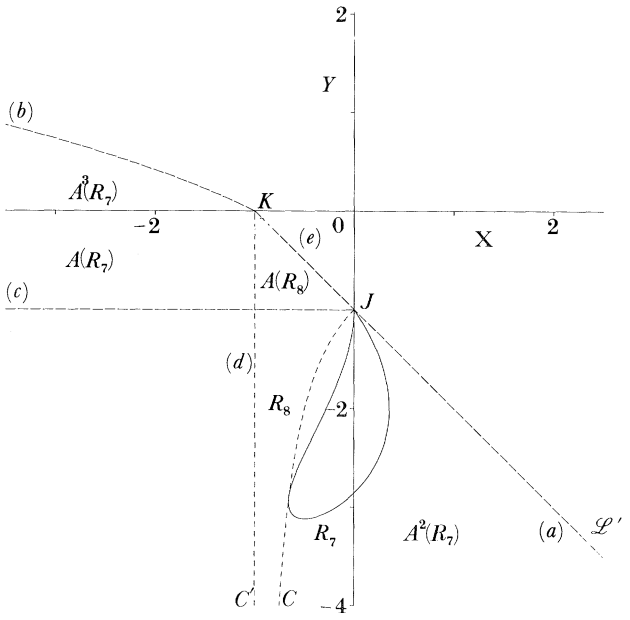

Figure 29. Partitioning of the outstanding regions. The partitioning is effected by means of just two subregions R_7 and R_8 together with images under A. (*a*) $A^2(\mathscr{N}_4)$, (*b*) $A^3(\mathscr{N}_4)$, (*c*) $A(\mathscr{N}_4)$, (*d*) $(\mathscr{N}_4)$, (*e*) $A^n(R_8)$, $n = 2, 3, \ldots$.

of these regions and some adjacent ones. The unbounded region may be seen to be composed wholly of iterates of regions R_7 and R_8. These latter regions are a partition of the semi-infinite strip $-1 < x < 0, y < -1$ divided by the curve $C: y = -1/(x+1)$, $y < -1$. Structure in R_8 is already known and all that is missing from R_7 is the interior of loops based at J. This will be determined first, and in the process, the corresponding loops in $A^2(R_7)$ become known, so that the totality of $A^2(R_7)$ is also thereby revealed. Having done this, all outstanding regions follow directly by iteration.

We turn again to the formation of loops based at J previously described in the text corresponding to figures 12 and 13 in §5.1. With reference to these figures, we recall that the first such loop along $W^u(Y_0)$ occurs in the fourth quadrant and is formed as the image of the arc Q_0J of $W^u(Y_0)$ in the third quadrant under the mapping B. The geometric effect of B in forming this loop can be loosely described as follows: firstly a compression of the whole arc Q_0J of the singular curve C along itself to the point J, thereby forming a loop, followed by reflection in the y-axis. Under the first process, all manifolds crossing C into the region Q_0JQ_0 have their intersection points with C mapped to J. The location of a line element meeting C determines the inclination of the image line element at J: elements near J have almost vertical images, elements along C far beyond Q_0 have images approaching J at nearly 45° to the axes. By continuity, points near C are attracted strongly towards J. Now the structure within the region Q_0JQ_0, bounded by $W^u(Y_0)$ and C, can be assembled from our previous results. This is shown in figure 30. It breaks into four subregions shown in figure 30*a* with structures indicated by figure 30*b*: $A(R_{2a})$ contains loops based at J (recall from §6.1 the role of l in separating loops based at J which cut C from those which do not); other structures may be inferred from figures 24 and 26*d* with 27 for the sector S. Applying B to this structure for the other subregions then yields a loop with

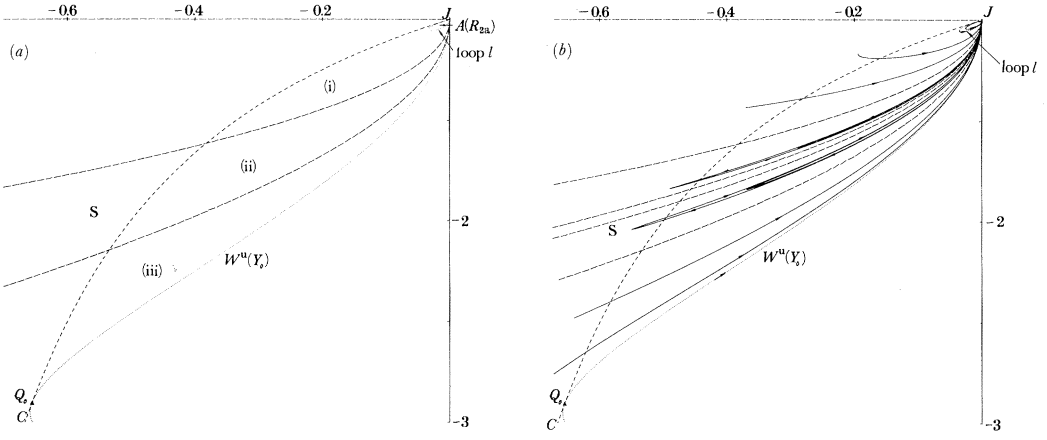

Figure 30. The preimage under B of the first loop of $W^u(Y_0)$: (a) partitioning into regions of distinct behaviour; (b) behaviour within the subregions. (i) $A(R_{3a}) \cap R_7$, (ii) $S \cap R_7$, (iii) $R_5 \cap R_7$.

subregions as in figure 31a. Both branches of the innermost loop $A^2(l)$, bounding $A^3(R_{2a})$, approach J vertically. All the other loops have one branch approaching J vertically and the other branch at some non-zero angle with the y-axis. Within the subregions $A^3(R_{2a})$, $A^2(A(R_{3a}) \cap R_7)$ and $A^2(R_5 \cap R_7)$, the structure is just that of nested loops, based at J, turning towards the y-axis, like $W^u(Y_0)$ itself. The image of the self-similar region (figure 30b) is more complicated. We recall that the self-similar region is composed of an infinite number of wedges each of which is foliated into nested loops. Thus its image is composed of an infinite number of subregions, each the image of a wedge. Let W be such a wedge. When $W \cap R_7$ only is considered (figure 31b), the outermost loops of W have their ends chopped off and so reduce to arcs connecting J to C, lying close to the boundary of W, while the innermost loops turn before C. Applying B, $W \cap R_7$ maps to an annulus-like region, illustrated in figure 31c, bounded by a pair of nested loops based at J. The outermost arcs lying within $W \cap R_7$ formed from the truncated loops of W map under B to loops similar to and close to this pair bounding the annulus. The innermost loops of $W \cap R_7$ also map to loops based at J. These, however, do not cycle round within the annular region: having emanated from J, they merely turn round within the annular region and return to J. $W \cap R_7$ and its image are shown in figure 31b, c in the case that W is the lowest wedge of the self-similar region of figure 30b. All other wedges have topologically equivalent images. Within the self-similar region S itself, the orientation of the loops changes as $W^u(P_1)$ is crossed, and there is a corresponding reversal in the images of these under B. Assembling the images of all these wedges and the other three subregions within the loop gives a complete qualitative description of the interior of the first loop of $W^u(Y_0)$ based at J.

Under further iteration by $B = A^2$, the first loop generates an infinite sequence of loops based at J accumulating on the y-axis alternating between the third and fourth quadrants. Since the first loop does not meet either of the singular curves C and C' of B nor any of their preimages, all iterates of the first loop are topologically equivalent. The main geometric points concerning these loops are that: (i) attraction towards the y axis is infinite at J (DB has eigenvalue = 0 there) and diminishes below J, so that subsequent loops are relatively more 'pinched' near J than away from J; (ii) the scale of the loops can be estimated from those shown in figure 13, noting that

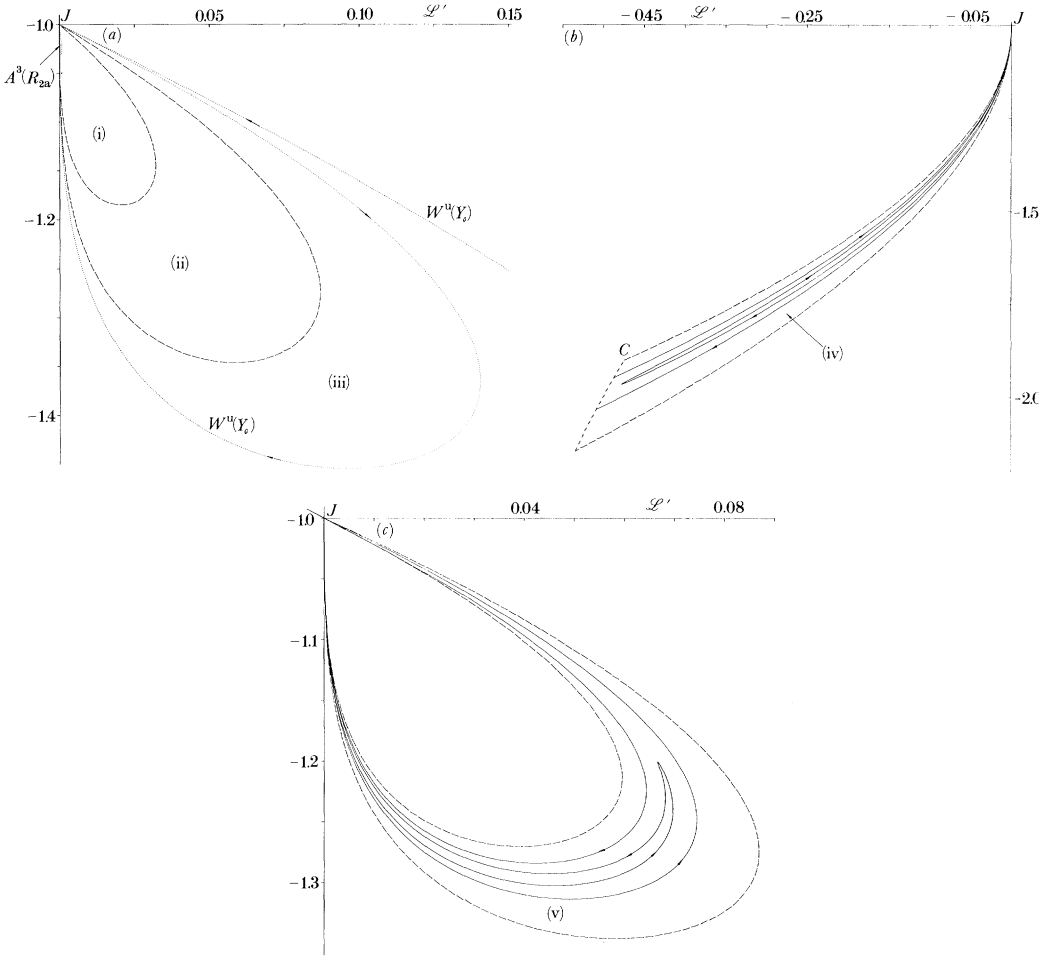

Figure 31. The first loop of $W^u(Y_0)$: (*a*) Partitioning: all subregions except $A^2(S \cap R_7)$ are foliated by nested loops based at J; (*c*) $A^2(S \cap R_7)$ is itself divided into an infinite sequence of regions similar to $A^2(W \cap R_7)$, whose construction follows from its preimage shown in (*b*). (i) $A^2(A(R_{3a}) \cap R_7$, (ii) $A^2(S \cap R_7)$, (iii) $A^2(R_5 \cap R_7)$, (iv) $W \cap R_7$, (v) $A^2(W \cap R_7)$.

points on these loops are attracted towards the y-axis below J along the stable manifolds of fixed points there and these manifolds are roughly inclined at 45° to the horizontal.

6.4. *Structure within the outstanding regions*

With the structure of the loops determined, we have a complete picture of the whole region enclosed by all branches of $W^u(Y_0)$ (see figure 13). In terms of figure 29, the regions R_7, R_8 and $A^2(R_7)$ are now all completely known, so that with one application of A, the regions $A(R_7)$, $A(R_8)$ and $A^3(R_7)$ may be constructed. The correspondence between $R_8 \cup R_7 \cup A^2(R_7)$ and its image under A is sketched in figure 32. The map A is singular on the left-most boundary of this domain, so to aid interpretation, we observe that a curve $y(x+1) = c$ has image $x = c$. Thus the curves PR and TR of figure 32*a* have straight line images $P'R'$ and $T'R'$ as in figure 32*b*. Figure 33*a* shows the division of $R_8 \cup R_7 \cup A^2(R_7)$ into regions of different invariant

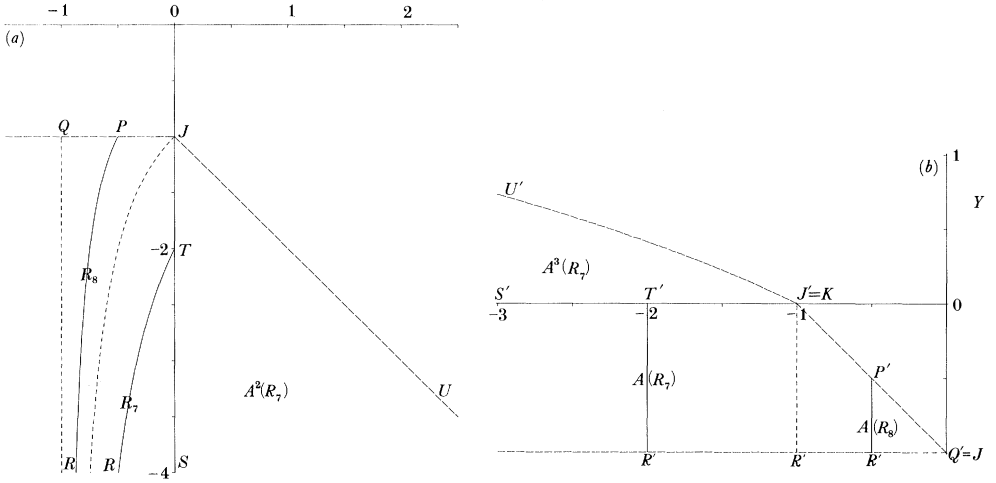

Figure 32. The regions $R_7, A^2(R_7), R_8$ and their images under A. Curves $y(x+1) = c$ shown in (a) have images $x = c$ shown in (b).

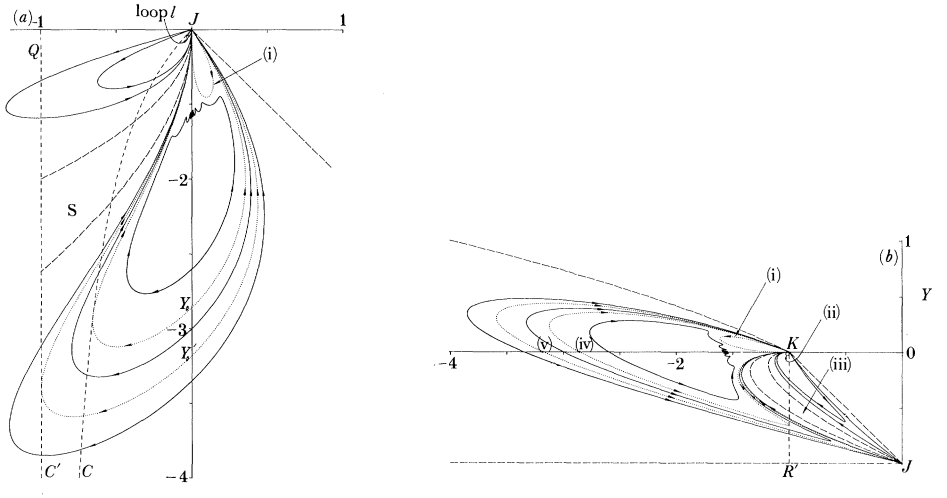

Figure 33. Manifold structure within regions $R_7, A^2(R_7), R_8$ and within the images of these regions under the mapping A. In (a) (i) is first loop of $W^u(Y_0)$. In (b) (i) first loop of $W^u(A(Y_0))$, (ii) loop $A(l)$, (iii) $A(S \cap (R_7 \cup R_8))$, (iv) $A(Y_0)$, (v) $A(Y_0')$.

curves. The regions are separated by dotted or broken lines while typical trajectories are shown solid. Such trajectories for S and the loops of $W^u(Y_0)$ are omitted because of their intricacy, and previous discussion should be consulted. When A is applied, a partitioning of the region $A(R_8) \cup A(R_7) \cup A^3(R_7)$ is obtained as shown in figure 33b. Recalling that A is singular on C' only, all structures within the domain are preserved topologically except where they intersect C': the image of such intersection points is the single point J. Further detailed qualitative features are now explained in the next paragraph.

Looking more closely at the various subregions, it follows from above, that the image of $W^u(Y_0)$ and its interior (including loops at J) is the topologically equivalent region enclosed by $W^u(A(Y_0))$ (and its attendant loops). A qualitative feel for the

shape of $W^u(A(Y_0))$ can be obtained from the following considerations. At $A(Y_0)$, $W^u(A(Y_0))$ must have the direction of the unstable eigenvector of DB, that is $(1+y_0, 1)$ where $y_0 = -2.8592161$. The next point to consider is the family of curves $y(x+1) =$ constant in a neighbourhood of Y_0. Such curves have a more positive gradient than $W^u(Y_0)$, but become less steeply inclined in the fourth quadrant. Thus $y(x+1) = y_0$ must meet $W^u(Y_0)$ at $Y_0 : (0, y_0)$ itself and again in the fourth quadrant. As a result, $W^u(A(Y_0))$ passes through $(y_0, 0)$ and additionally meets the line $x = y_0$ somewhere in the second quadrant. Curves $y(x+1) = c$ with c slightly more negative than y_0 cut $W^u(Y_0)$ twice in the fourth quadrant, but as c is decreased, there is eventually a c_0 such that $y(x+1) = c_0$ only meets $W^u(Y_0)$ tangentially in the fourth quadrant. In consequence of this, $W^u(A(Y_0))$ extends leftwards from $A(Y_0)$ into the second quadrant as far as $x = c_0$, where it turns back and then runs into K. Considering the arc of $W^u(Y_0)$ in the third quadrant between Y_0 and the singular curve C, this arc cuts each curve $y(x+1) = c, y_0 < c < -1$ exactly once. The image of this portion of $W^u(A(Y_0))$ therefore moves monotonically to the right as far as the line $x = -1$ (the line KR' in figure 33*b*). It touches this line tangentially. Finally, the arc of $W^u(Y_0)$ between the tangency point with C and the point J meets each curve $y(x+1) = c$ twice for $c_1 < c < -1$, where c_1 is a constant slightly less than -1. As a result, the image of this arc extends from the tangency point with KR' leftward as far as $x = c_1$ before turning and running into K parallel to the x-axis. Similar considerations allow inferences to be drawn about the qualitative shapes of other image curves, but we omit the details. The pinched annular region between $W^u(Y_0)$ and $W^u(Y_0')$ maps to the pinched annular region between $W^u(A(Y_0))$ and $W^u(A(Y_0'))$. The latter manifold has connected branches $KA(Y_0')J$ and JK. These meet tangentially at J because, under the map A, location on C' determines orientation only at J, and the corresponding branches of $W^u(Y_0')$ both meet C' at the same point. Manifolds in the pinched annular region between $W^u(Y_0)$ and $W^u(Y_0')$ cross C twice, but do not extend to C'. In consequence, the image of such a manifold cuts KR' twice, possessing an arc within the triangle $KR'J$, but which does not extend to J. An example of this is provided in figure 33*b* by $W^u(X)$ where $X = (-3, 0)$ which lies between $A(Y_0')$ and $A(Y_0)$. For a point Y below Y_0', $W^u(Y) \cap (R_8 \cup R_7 \cup A^2(R_7))$ has two connected components: the first through Y itself extending to C' in one direction and J in the other; the second connecting C' to J in the region between sector S and $W^u(Y_0')$. The image of the first component is a 'long' arc through $A(Y)$ on the negative x-axis, which extends to K above this axis and to J below it. It is the outermost solid curve of figure 33*b*. The second component has an image from J to K shown as the solid curve below the crescent shaped region labelled $A(S \cap (R_7 \cup R_8))$. This crescent shaped region is itself the image of the self-similar sector S restricted to $R_7 \cup R_8$. When A is applied, the end of this restricted sector lying on C' is compressed to the point K. The resulting crescent shape has a structure analogous to that described in the discussion of the first loop of $W^u(Y_0)$ (see figures 30 and 31): the crescent shape is divided into an infinite sequence of subcrescents, each of which has a structure similar to the region $A^2(W \cap R_7)$ shown in figure 31*c*. Here, however, each subcrescent region does not loop back on itself (as does $A^2(W \cap R_7)$), but extends from K to J, and possesses an innermost internal structure of nested loops based at K, flanked by arcs between K and J.

In the third quadrant, above the sector S of figure 33*a*, there are nested loops based at J. The loop l, shown by the solid line, lies wholly below C (see discussion of figure 23*a*), and thus has an image $A(l)$ completely to the left of KR'. This loop l has

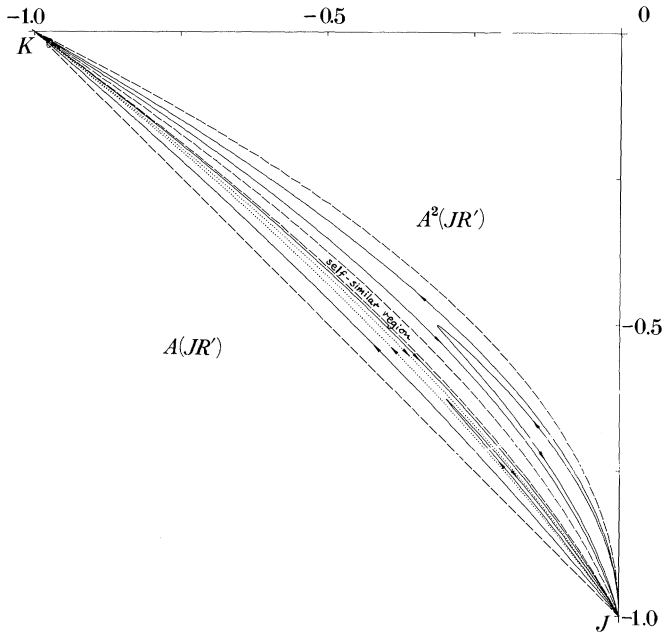

Figure 34. Manifold structure within the region $A^2(R_8)$.

branches approaching J tangentially to C and tangentially to the y-axis. Consequently, its image $A(l)$ approaches K tangentially to KR' and the x-axis respectively. If we recall that l is part of $W^u(A(Y_2'))$, it follows that $A(l)$ is part of $W^u(A^2(Y_2')) = W^u(B(Y_2')) = W^u(Y_2')$, and we can then identify $A(l)$ as the dotted loop shown in the inset of figure 21*a*. The nested loops inside l map to analogous image loops (also shown in figure 21*a* in the third quadrant relative to K). A loop exterior to l in figure 33*a* has an image that depends on whether or not it extends as far as C'. If it does not, the loop has one connected component which crosses C. Its image is therefore a loop at K, exterior to $A(l)$, which crosses from one side of KR' to the other. If a loop exterior to l does extend to C', then its restriction to $R_8 \cup R_7$ has two connected components, one of which emanates leftward from J extending to C', and the other returning to J from C', crossing C in the process. The image of this consists of an arc from K to J lying wholly in $x > -1$ together with a second arc from J to K which cuts KR' before turning to approach K parallel to the x-axis. These are the uppermost and second uppermost broken lines respectively leading to and extending from J in figure 33*b*.

There remains just the behaviour in the triangle KOJ of figure 34 to be ascertained. This triangle contains all the image regions of $A(R_8)$ under iteration by A. The structure of $A(R_8)$, that is the structure within triangle $KR'J$ of figure 33*b* follows from the previous discussion. The image under A of $A(R_8)$ is the lune-shaped region shown in figure 34. This is bounded below by the line KJ, which is the image of $R'J$ bounding $A(R_8)$, and above by the curved arc $KJ: x = -(1+y)^2, -1 < y < 0$ which is the image of the line KJ bounding $A(R_8)$. Thus the boundary of $A^2(R_8)$ consists of $A(R'J)$ and $A^2(R'J)$. Construction of the interior follows from a geometric interpretation of applying A to $KR'J$ in figure 33*b*: there is initially a nonlinear shearing upwards under which J and K remain fixed, but all points within $R'K$ are compressed to K, while $R'J$ moves up to the line KJ and the line KJ becomes convex

upwards. The resulting region is then reflected in $y = x$, so that K and J are interchanged. Following the various subregions of $KR'J$ under this process yields a partitioning of $A^2(R_8)$ as shown in figure 34. The arcs JK and loops based at J in figure 34 all follow directly from the corresponding arcs in the region $KR'J$ of figure 33*b* under the geometric process just described, whereas the self-similar region contains an infinite sequence of sub-lunes, each of which has an innermost structure of nested loops based at J surrounded by arcs connecting J and K (see figure 31*c*). Under further applications of A, a sequence of increasingly narrow crescent-shaped regions $A^n(R_8), n = 3, 4, 5, \ldots$ results, bounded by $A^{n-1}(JR')$ and $A^n(JR')$. These are all topologically equivalent, have alternating orientation, and accumulate on the interval KOJ, being attracted by the fixed points there. As the boundary $A^n(JR')$ of $A^n(R_8)$ is the image under A of its other boundary, the entirety of the triangle KOJ is thus described. This completes description of behaviour throughout the plane.

6.5. *Non-existence of orbits with periods greater than 3*

Knowledge of the overall structure of the invariant manifolds now enables us to demonstrate that there are no periodic points other than the ones already encountered, and thus, that there are no orbits of period greater than three. The method used has elements of the ideas of symbolic dynamics (Guckenheimer & Holmes 1983). If a point P has period p under A and lies in a region R, then, of necessity $R \cap A^p(R) \neq 0$. This condition rapidly rules out the existence of periodic points in many of the regions considered earlier. Combined with other information on the nature of the invariant manifolds, all the remaining regions may then be eliminated. Below, we list the various regions (taken to be open) and their iterates together with a relevant figure number. Where necessary, additional reasons are given for the non-existence of periodic orbits.

(i) $R_0 \to A(R_0) \to R_0$ (figure 23*a*). In both R_0 and $A(R_0)$, iterates move upward and to the right under the action of A^2 (see §2), so that no periodic points exist in these regions.

(ii) $R_1 \to A(R_1) \to R_1$ (figure 23*a*). In both R_1 and $A(R_1)$, iterates move downward and to the left under the action of A^2 (see §5), hence no periodic points.

(iii) $R_2 \to A(R_2) \to R_2 \cup R_{2a} \cup R_{2b}$ (figure 23*a*). R_2, however, is composed wholly of portions of unstable manifolds $W^u(Y)$ and all such points eventually escape from R_2. Thus it suffices to consider iterates of R_{2a} and R_{2b}: $R_{2a} \to A(R_{2a}) \to$ an infinite sequence of disjoint loops based at J and K; R_{2b} is similar.

(iv) $R_3 \to A(R_3) \to R_3 \cup R_{3a}$ (figure 23*a*). As for R_2, all points of R_3 eventually escape from R_3 so it suffices to consider R_{3a}. $R_{3a} \to A(R_{3a}) = \tilde{R}_{3a} \cup (A(R_{3a}) \cap R_8) \cup (A(R_{3a}) \cap R_7)$ (figures 26*b*, 29). $\tilde{R}_{3a} \to$ self-similar sector S (figure 26), discussed below. $A(R_{3a}) \cap R_8 \to$ disjoint lunes $A^n(R_8), n = 1, 2, 3, \ldots$ (figure 34). $A(R_{3a}) \cap R_7 \to$ an infinite sequence of disjoint loops based at J and K (figure 31*a*).

(v) $R_4 \to$ self-similar sector S, discussed below.

(vi) Self-similar sector S. We may decompose S as $S = \bigcup_{n=1}^{\infty} A^{3n}(\mathrm{cl}\,(\tilde{R}_{3a}) \cup \mathrm{cl}\,(R_4))$ (figure 26), where cl denotes the closure. The wedge-shaped subregions $A^{3n}(\mathrm{cl}\,(\tilde{R}_{3a}))$ are all disjoint, so that if a point P other than J lies in one of these subregions, it cannot lie in any of its iterates, and so cannot be periodic. The regions $A^{3n}(\mathrm{cl}\,(R_4))$ are similar. The only remaining points of S are P_1 and $W^u(P_1) \cap S$. P_1 is periodic; under A^3, all points of $W^u(P_1) \cap S$ are repelled from P_1, and so cannot be periodic.

(vii) We partition R_7 into $R_{7a} \cup R_{7b} \cup R_{7c}$ (figure 29), where R_{7a} is the portion of R_7 between $W^u(Y_0)$ and the y-axis, R_{7b} is the portion of R_7 above R_{7a}, R_{7c} is the portion

of R_7 below R_{7a}. All points of R_{7a} are attracted towards fixed points on the y-axis (figure 13). All points of R_{7b} are mapped to sequences of disjoint loops based at J and K (figures 30*b*, 31). Region R_{7c} is composed wholly of unstable manifolds $W^u(Y)$ (figure 22) so that all points of R_{7c} eventually escape from R_{7c} into $R_8 \cup R_4 \cup R_{7b}$ initially. The iterates of R_4 and R_{7b} are discussed above, and those of R_8 are listed below. It follows that $R_7, A(R_7), A^2(R_7), A^3(R_7)$ (see figure 29) and any other distinct iterates of R_7 are all devoid of periodic points.

(viii) The only outstanding region is R_8, which maps to the infinite sequence of disjoint lunes $A^n(R_8), n = 1, 2, \ldots$.

We have shown that none of the regions considered above contains any periodic points other than those previously found. We have omitted to discuss the boundaries of some of these regions, but the same conclusion may be drawn by using similar methods.

I record my gratitude to my colleagues Dr J. G. Byatt-Smith, Dr A. M. Davie and Dr D. C. Heggie for many useful conversations and helpful suggestions.

References

Collet, P. & Eckmann, J.-P. 1980 *Iterated maps on the interval as dynamical systems*. (*Progress in physics*, vol. 1.) Boston: Birkhauser.

Grossman, J. W. 1986 *Math. Intelligencer* **8** (1), 31.

Guckenheimer, J. & Holmes, P. 1983 *Nonlinear oscillations, dynamical systems and bifurcations of vector fields*. Berlin: Springer-Verlag.

Hénon, M. 1976 A two-dimensional mapping with a strange attractor. *Communs math. Phys.* **50**, 60–77.

Janssen, A. J. E. M. & Tjaden, D. L. A. 1987 *Math. Intelligencer* **9** (3), pp. 41–43.

Metropolis, N., Stein, M. L. & Stein, P. R. 1973 On finite limit sets for transformations on the unit interval. *J. Comb. Theory* A **15**, 25–44.

Šarkovskii, A. N. 1964 Coexistence of cycles of a continuous map of a line into itself. *Ukr. Mat. Z.* **16**, 61–71.

Shub, M. 1987 *Global stability of dynamical systems*. Berlin: Springer-Verlag.

Strang, G. 1986 *Introduction to applied mathematics*. Wellesley: Wellesley–Cambridge.

Received 1 November 1989; accepted 5 January 1990

PHILOSOPHICAL TRANSACTIONS OF THE ROYAL SOCIETY A MATHEMATICAL, PHYSICAL & ENGINEERING SCIENCES